uc3m | Universidad Carlos III de Madrid

e-Archivo

This is a postprint version of the following published document:

Palanca, M., Marco, M., Ruspi, M. L., & Cristofolini, L. (2018). Full-field strain distribution in multi-vertebra spine segments: an in vitro application of Digital Image Correlation. Medical Engineering & Phisics, 52, 76–83.

DOI: https://doi.org/10.1016/j.medengphy.2017.11.003

© 2017 IPEM. Published by Elsevier Ltd. All rights reserved.

This work is licensed under a Creative Commons Attribution-NonCommercial-NoDerivatives 4.0 International License.

Full-field strain distribution in multi-vertebra spine segments:

An *in vitro* application of Digital Image Correlation

Marco Palanca
School of Engineering and Architecture, Alma Mater Studiorum – Università di Bologna
Via Terracini 28, 40131, Bologna (Italy)
marco.palanca2@unibo.it

Miguel Marco
Department of Mechanical Engineering, Universidad Carlos III de Madrid
Avd. de la Universidad, 30. 28911 Leganés (Madrid) España
mimarcoe@ing.uc3m.es

Maria Luisa Ruspi
School of Engineering and Architecture, Alma Mater Studiorum – Università di Bologna
Via Terracini 28, 40131, Bologna (Italy)
marialuisa.ruspi2@unibo.it

Luca Cristofolini*
Department of Industrial Engineering, School of Engineering and Architecture, Alma Mater Studiorum – Università di Bologna
Viale Risorgimento 2, 40136, Bologna (Italy)
luca.cristofolini@unibo.it

*Corresponding author

Abstract

The biomechanics of the spine is experimentally assessed in terms of range of motion and overall stiffness. Quantification of the surface strain distribution is currently limited either to the vertebrae or the discs, whereas a full-field approach to measure the strain distribution in a multi-vertebra segment is currently missing. The aim of this work was to explore the feasibility of using Digital Image Correlation (DIC) to measure the strain distribution simultaneously on the vertebral bodies and the intervertebral discs of spine segments in different loading configurations.

Three porcine spine segments were tested. A white-on-black speckle pattern was prepared which covered the hard and soft tissues. Two different loading configurations (flexion and lateral bending) were reproduced, while two sides of the spine were analyzed with DIC.

Measurements were successfully performed on the entire region of interest of all specimens, in both configurations. The DIC analysis highlighted the strain gradients present on the spine segments including tension and compression associated with bending, the direction of principal strains in the different regions, as well as bulging of the discs under compression. Strains of tens of thousands microstrain were measured in the discs, and below 2000 microstrain in the bone.

This work showed the feasibility of applying DIC on spine segments including hard and soft tissues. It also highlights the need for a full-field investigation, because of the strain inhomogeneity in the vertebrae and discs.

Keywords: Biomechanics; Spine segment; Full-field strain measurement with Digital Image Correlation; Feasibility study; Intervertebral Discs; Vertebrae.

1. Introduction

The spine consists in a sequence of hard (vertebrae) and soft tissue (intervertebral discs), stabilized by ligaments. Spine characterization is a fundamental challenge in biomechanics because it could help engineers and clinicians to better understand physiological/pathological conditions, and to design better implants [1, 2].

Spine segments have often been investigated *in vitro* [3-7]. In such experiments either known motions are imposed to measure the structural stiffness [8-10], or known loads are applied to measure the range of motion[11-13]. From these tests, structural properties and behaviour of the spine segment as a whole is assessed. Only in few cases the local strain distribution has been measured. However, such experiments focused separately either on the vertebra or on the intervertebral disc. Strain in the vertebra has been measured by means of strain gauges [14-17]; this provided accurate measurements, but was limited to the area of application of the strain gauges. The reinforcement effect of strain gauges can be significant (up to 9%) [14, 18, 19]. Measuring the local strain in the intervertebral disc is even more difficult, due to the intrinsic nature of the disc itself (low stiffness). One of the first measurements of the strain on the outer part of the disc (*annulus fibrosus*) was based on stereo-photogrammetry and covered a limited portion of the disc [20]. More recently, the entire disc surface was investigated (excluding the adjacent vertebrae), using digital image correlation (DIC) [21]. A method to explore the strain field on spine segments with large in-plane and out-of-plane deformations is missing.

The aim of this work was to explore the feasibility of using DIC to measure the full-field strain distribution simultaneously on the vertebral bodies and intervertebral discs of thoracolumbar spine segments in different loading configurations. Specifically, the following research questions were addressed:

- The feasibility of applying a speckle pattern with sufficient contrast for the correlation algorithm, that should not become damaged when the specimen was kept hydrated;

- The robustness of the pattern to withstand the large deformations expected in the soft tissue (up to 100000 microstrain) for up to 50 cycles;
- The procedure must allow measuring the small deformations expected in bone (of the order of 2000 microstrain) with acceptable errors (not exceeding 200 microstrain);
- The possibility of measuring strains in specimens undergoing relatively large in-plane (up to 3 mm) and out-of-plane (7 mm) displacements, while correlating at least 90% of the region of interest.

2. Material and methods

2.1 Specimen and pattern preparation

For ethical reasons, in this methodological work porcine spine segments from the slaughterhouse were preferred. The three animals were female, of the same breed, approximately 9 months old and approximately 100 kg at sacrifice. The segments consisted of four thoracolumbar vertebrae (T7-T10/T11-T14/L2-L5) selected for resemblance in terms of ranges of motion and dimensions [22-24]. The specimens were kept hydrated, and stored at -28°C to avoid alteration of the mechanical properties.

The ribs, the muscles, the anterior longitudinal ligament, and the periosteum were carefully removed using surgical tools. The interspinous, supraspinous and posterior longitudinal ligaments, and the capsules were left intact in order to preserve the natural kinematics. The specimens were aligned so that the middle disc of each segment was aligned horizontally in the frontal and lateral views [25]. In this configuration, two pots of poly-methyl-methacrylate were created parallel to one another, where the upper half of the most cranial vertebra and the lower half of the most caudal vertebra, were embedded (Fig. 1).

In order to use DIC to make measurement on the spine segments (both the vertebrae and the intervertebral discs), a high-contrast white-on-black speckle pattern [26, 27] was prepared. The spine segments were first stained with a dark background (a solution of 4 g of methylene-blue per 100 ml of water) [28, 29]. Two applications were required for the intervertebral discs and three for

the vertebrae to obtain a uniform background. Dying was preferred, rather than surface painting, as a layer of paint would crumble and crack due to the large deformations of the soft tissues.

The speckle pattern was applied with paint instead of using a powder, as was done previously [26]. This allows avoiding artifacts as the dots can strain during the test (unlike powder grains). Furthermore, paint dots resist to saline solution without damage, allowing specimen hydration and storage. A white water-based paint (Q250201 Bianco Opaco, Chrèon, Italy) was diluted at 40% with water and sprayed using an airbrush-airgun (AZ3 HTE 2, nozzle 1.8 mm, Antes Iwata, Italy) to prepare a white speckle pattern with the qualitative and quantitative requirements described in [30]. The spraying distance (300 mm) and the pressure (1000 kPa) were optimized to obtain the desired dot size, and minimize the scatter of dot dimension [35]. The actual size of the speckle dots was measured in the 2D digital images (acquired by DIC system) of the ROI through a custom script developed for this work. The speckles had a dimension of 6 pixels (average 0.18 mm with a standard deviation of 0.18 mm), larger than the minimum recommended size while the facet were sufficiently large compared to the speckle size [30].

The specimens were soaked in saline solution before the tests.

2.2 Mechanical Testing

The specimens were loaded using a uniaxial servo-hydraulic testing machine (8032, Instron, UK) in displacement control. In order to avoid transmission of any undesired component of load, free rotation of the loading plate was allowed by means of a ball joint, while free horizontal translations were granted by means of two low-friction orthogonal linear bearings.

In order to assess the feasibility of measuring strains on such complex specimens, two different loading configurations were simulated, which are frequently investigated in the literature [31] (Fig. 2):

- Flexion: the vertical force had an anterior offset equal to the 20% of the antero-posterior depth of the central intervertebral disc;

- Lateral bending: the vertical force had a lateral offset (both towards right and left) equal to the 20% of the coronal width of the central intervertebral disc.

Ten preconditioning cycles were applied between 0 and 1.0 mm of compression, at 0.5 Hz. A compression of 3.0 mm was applied for each loading configuration in 0.1 mm steps, while DIC images were acquired at each step (see below). This value of compression was based on preliminary tests to reach typical strains associate to physiological loads [32, 33] to prevent damage of the specimens. These loading configurations did not aim to mimic any specific motor task.

2.3 Digital Image Correlation

A commercial 3D-DIC system (Q400, Dantec Dynamics, Denmark) with directional custom designed arrays of LEDs (10000 lumen in total) was used. Images were acquired by two cameras (5MegaPixels, 2440x2050 pixels, 8-bit) equipped with high-quality metrology-standard 35 mm lens (Apo-Xenoplan 1.8/35, Schneider-Kreuznach, Germany; 135 mm equivalent) for a stereoscopic view. Due to the curvature of the vertebral bodies and discs, the cameras were positioned at a distance of 260 mm from the specimen and vertically to maximize the area framed by both cameras (Fig. 2).

The field of view was set to 70 mm by 60 mm (resulting in a pixel size of 28 micrometers), with depth of field of 20 mm (lens aperture f/16). The field of view was wide enough to frame the entire region of interest (ROI): the central intervertebral disc and the two adjacent vertebrae.

To explore the possibility of assessing the different sides of the spine, two different acquisitions were performed for each loading configuration and each specimen:

- Frontal view: the cameras pointed the anterior wall of the spine segment;
- Lateral view: the cameras pointed the lateral side (either right or left) of the spine segment.

During the mechanical tests, series of images were acquired starting from the unloaded condition (reference step) and every 0.1 mm step of compression.

The correlation was performed with Istra-4D (v.4.3.1, Dantec Dynamics, Denmark) using the following parameters (Fig. 1):

a) Facet size: 33 pixels;
b) Grid spacing: 19 pixels;
c) Contour smoothing: local regression with a kernel size of 5x5;

It is not possible to exactly quantify the measurement spatial resolution due to the nonlinearity of the smoothing process. With the settings used, a spatial resolution better than 3 mm was estimated (comparable with the typical dimension of the strain gauges used in biomechanical field [14]).

Finally, the maximum (ε_1) and minimum (ε_2) principal strains were evaluated.

2.4 Optimization and error analysis

As DIC relies on a complex preparation, acquisition and analysis, its accuracy and precision cannot be taken from granted. We capitalized on past experience on optimization of pattern preparation [28] [35], image acquisition and correlation parameters [34] (see 2.1 and 2.3).
Before each session, calibration was performed using a proprietary calibration target (Mod. Al4-BMB-9x9, Dantec Dynamics): 3D-residuum values from 0.031 to 0.173. It is a proprietary procedure and it consists in acquiring a series of images of the target calibration in different orientations to define the physical dimensions of the measurement volume, the correction of the distortions due to lens and the compensation of the parallax effects.

An optimization and validation of the system was preliminarily performed [34] to find the best compromise between the uncertainties and DIC parameters. A pair of images of the unloaded segments were captured for each specimen and analyzed with the optimal hardware and software settings in order to assess the measurement uncertainties in a known configuration (zero-strain). Being in a zero-strain configuration, any strain different from zero was accounted as measurement error. The Kolmogorov-Smirnov test was used to check that the errors followed a Gaussian distribution. The systematic and random errors [34] were computed for each specimen and for each view as the average and the standard deviation of ε_1 and ε_2.

3. Results

Measurements were successfully performed on all specimens, over the entire region of interest in both the frontal and sagittal view, for both loading configurations, during the entire tests. Similar strain distributions were found in the three specimens. The different tissues were easily identified observing the physical specimens and the images acquired by the cameras. The evolution of the strain distribution during load application (Fig. 3) is visible in the videos in the Supplementary Material.

3.1 Strain error

In the zero-strain test, the apparent strains followed a Gaussian distribution (Kolmogorov-Smirnov). As expected, the largest component of error was the random error, and it never exceeded 190 microstrain.

3.2 Flexion – Frontal view

During flexion, at most 4.4% (worst specimen) of the ROI in the frontal view lost correlation between the first and the last step. The discs underwent larger deformations compared to the vertebral bone (Fig. 4). The strain in the discs followed a strain gradient, with peaks in the central portion. In the discs, ε_1 was on the order of +20000 microstrain (aligned circumferentially) and ε_2 was of the order of -40000 microstrain (aligned axially).

The vertebrae had lower strains: peak on the order of +500 microstrain for the ε_1 and around -1500 microstrain for ε_2. The two regions cranial and caudal to the intervertebral discs with larger strain show the large deformation of the growth plates.

3.3 Flexion – lateral view

During flexion, at most 5.7% (worst specimen) of the ROI in the lateral view lost correlation between the first and the last step. The discs presented a strain gradient: they were more deformed in tension in the posterior than in the anterior side (Fig. 4). ε_1 on the intervertebral discs varied between +12000

180 microstrain (anterior side) and +87000 microstrain (posterior side). ε_2 followed
181 a similar gradient, from -87000 microstrain (anterior) to -18000 microstrain
182 (posterior). The direction of ε_1 changed from circumferential (anterior side), to
183 axial (posterior). Therefore, in flexion the discs tended to bulge in the anterior
184 part, and to stretch in the posterior side.

185 The vertebral body experienced lower strains: below +600 microstrain for ε_1 and
186 -1500 microstrain for ε_2.

187 ***3.4 Lateral bending – frontal view***

188 During lateral bending, at most 1.5% (worst specimen) of the ROI in the frontal
189 view lost correlation between the first and the last step. Lateral bending was
190 applied both towards the right and the left sides, to all specimens: the outputs, in
191 terms of strain distribution on intervertebral discs and vertebrae were
192 symmetrical. The discs showed tension and compression respectively on the left
193 and right sides, depending on the direction of the imposed bending (Fig. 4). ε_1
194 varied between +6000 microstrain (compressed side) and +143000 microstrain
195 (stretched side). ε_2 were varied from -85000 microstrain (compressed side) to
196 +12000 microstrain (stretched side). The orientation of ε_1 changed from
197 circumferential on the compressed side, to axial on the stretched side.

198 The vertebrae had lower strains than the discs: ε_1 were lower than 500
199 microstrain and ε_2 did not exceed -1700 microstrain. In this configuration, as in
200 flexion, it was possible to observe both tension (ε_1 aligned with the vertebral
201 axis) and compression (ε_2 circumferentially) in the growth plates.

202 ***3.5 Lateral bending – lateral view***

203 During lateral bending, at most 5.2% (worst specimen) of the ROI in the lateral
204 view lost correlation between the first and the last step. The strains on the discs
205 were rather uniformly distributed compared with the other tests (Fig.4). When
206 the side in compression was observed, ε_1 in the disc were of the order of +40000
207 microstrain, and ε_2 of the order of -60000 microstrain.

The vertebral body had lower strains than the discs: ε_1 were lower than 700 microstrain and the ε_2 did not exceed -1400 microstrain.

4. Discussion

The main aim of this work was to develop a procedure to measure the strain distribution on thoracolumbar spine segments [36] simultaneously on hard tissues (the vertebrae) and soft tissues (the intervertebral discs) by means 3D-DIC [30]. Two different loading configurations frequently found in the literature [6, 11-13] were explored. The specimens were observed both frontally and laterally.

The results of this work showed the technical feasibility of quantifying the full-field strain distribution (small and large deformations) over multi-vertebra spine segments during the mechanical tests. The measured strain distributions proved to be highly inhomogeneous, confirming the importance of investigating the spine using a full-field tool to complement the evaluation of the range of motion and stiffness performed in the past.

The correlation was satisfactory throughout the tests, even if large deformations and displacements were involved. The correlated surface covered the ROI, with a loss of correlation lower than 5.7% of the initial correlated surface. Generally, the noise originating from the camera sensors, sub-optimal speckle dots, poor illumination, and bad speckle framing can contribute to loss of correlation. Here, the leakage of fluids from the vertebral body under load, which is an inherent phenomenon when testing fresh tissue, increased the loss of correlation. Additionally, the out-of-plane movements (7 mm) of the postero-lateral elements (capsule) caused some subsets to be out-of-focus in the lateral view. While DIC often has some un-correlated gaps, other measurement techniques such as strain gauges simply measure strains in selected points, and ignore the rest of the surface.

The prepared white-on-black pattern confirmed its suitability both for hard and soft tissues [28]. In fact, the background, prepared with methylene-blue, did not

crack during the tests, while the white dots remained sharp and adherent to the specimen's surface.

A compromise was sought between reduction of measurement uncertainty and spatial resolution. The hardware (camera resolution, lenses, field of view) and software parameters (facet size, grid spacing, contour smoothing) provided a measurement spatial resolution better then 3 mm. This is comparable with the grid length of the strain gauges typically used in these applications (1-5 mm) [37-40]. The strain measurement uncertainties (below 180 microstrain) were acceptable for biomechanical purposes. Such uncertainties would not prevent detecting failure of the bone (around 10000 microstrain [32]), as well as strain associated to physiological loads (1000-2000 microstrain [41]). The same considerations are confirmed for the intervertebral discs: as the failure strain is around 250000 microstrain [20], and the physiological strain is below 150000 microstrain [33].

The evaluated strains confirmed the expected trends in all performed tests: larger strains were measured in the intervertebral discs (in the order tens thousands microstrain), lower strains in the vertebrae (below 2000 microstrain). Such strain gradients are consistent with the expected biomechanics of the spine [4]. DIC discriminated the portion of the discs subjected to tension/compression, with the expected orientation of the principal strains. In the compressed side of the discs the minimum principal strains were axial, as expected; the maximum principal strains were larger in absolute value than the minimum ones, and had a transversal orientation.

The combination of the prepared pattern, selected software parameters, and hardware allowed recognizing the deformation on the growth plates of the vertebrae. Because of the spine specimens came from skeletally immature animals [42] the growth plates were not closed and therefore were subjected to larger deformation compared to the vertebral body. This was serendipity and would otherwise be impossible to observe with traditional surface measurement technique such as strain gauges.

Usually, *in vitro* spine segments have been investigated in terms of range of intersegmental motion [6, 12, 13, 43] and overall stiffness [11, 13, 44, 45]. In other works, the spine was investigated measuring local deformation either in the vertebrae or in the intervertebral discs. In the vertebrae, strains have been evaluated using strain gauges, which provide point-wise measurements. At the same time, strain gauges do cause reinforcement, especially on thin osteoporotic tissues [14, 15]. Otherwise, the vertebrae have been studied using DIC but without evaluating the contiguous discs [34, 46]. Conventional strain gauges cannot be used on the discs due to their low elastic modulus. Strain measurement is possible with optical methods [20, 21]. In the work of Stokes *et al.* [20] the deformation on a small portion of the intervertebral disc was evaluated by photogrammetry adhering small optical markers. Heuer *et al*. [47] developed a method based on laser scanning device to evaluate the strain distribution on intervertebral discs. In this case, the strain uncertainty (<1600 microstrain) would not allow measuring strain on hard tissue as vertebra. Moreover, the duration of the scan (4 seconds), constrains the applicability to quasi-static applications. In the work of Spera *et al*. [21] strain was measured only on the discs using DIC. They used coffee powder: as the coffee grains themselves are not deformable as the paint-dots, this can result in large noise, apparent strain and loss of correlation.

A work [48] focused on the strain distribution on spine segments. High-speed 3D-DIC was used to evaluate the strains on the anterior side of porcine cervical spine segments in axial impacts. In contrast, the present work aims to explore the feasibility of the measurement under large deformation, directed out-of-plane.

A limitation of this work could be the use of young porcine spine instead of human spine. This choice was motivated by ethical considerations. The porcine spines are different from the human ones but are valid models [22, 24] to demonstrate the feasibility of this novel approach.

In this work, a quite standard but relatively simple configuration of 3D-DIC was used. Array of cameras can be used to acquire 360° of the whole spine in order to obtain a complete description of the strain maps.

The applied loading configurations were not intended to replicate any specific physiological motor task, but included separate components of load which are present in physiological motor tasks (flexion and lateral bending) and which are typically found in spine biomechanics [31] as main causes of spine degeneration [49]. This study did not cover other types of loading such as torsion.

The strains were evaluated only on the surface of the specimens. Digital Volume Correlation (DVC) [50] has the potentiality to evaluate the strain within the vertebral bone [51-53]. Nevertheless, applicability of DVC is limited due to the slow tomographic image acquisition.

5. Conclusion

This work showed that by applying an adequate speckle pattern and selecting optimal DIC parameters, the full-field strain distribution could be evaluated on a complex structure (soft and hard tissues) such as a spine segment. This full-field measurement would allow assessing the strain distribution, determining the alignment of principal strains, and identify stress concentrators. This opens the way to a new method of investigation of the spine, involving new possible applications for basic biomechanics research and clinical innovations. DIC-based experimental measurements could be combined with numerical models in an inverse approach to measure (identify) the local tissue properties, including anisotropy. Furthermore, the use of DIC will help elucidate the damage and failure mechanism of the spine. DIC can also be used to investigate and improve different surgical techniques and spine fixation devices.

Conflict of Interest Statement

None

Acknowledgements

The authors would like to thank Remo Antelli for donating the porcine spines, Thorsten Siebert (Dantec Dynamics, Denmark) for the support with DIC software, and the students for the help in the preparation of the specimens (Kamila Ożóg, Büşra Savaş, Alessio Amicone).

Competing interests:

None declared

Funding:

None

Ethical approval:

Tissue specimens (porcine spines) were obtained as a side-product through the food chain from animals that have been bred and sacrificed for alimentation purposes. No animal was specifically bred or sacrificed for this study. The Biomechanics laboratory at UNIBO meets all the Italian regulations concerning research, safety in the working environment, handling, storing, testing and disposal of animal and human tissue samples. All the research was carried out in accordance with the National and local regulations guidelines and, in accordance with the EU Directive 2010/63/EU.

Bibliography

[1] Smith JS, Sansur CA, Donaldson WF, 3rd, Perra JH, Mudiyam R, Choma TJ, et al. Short-term morbidity and mortality associated with correction of thoracolumbar fixed sagittal plane deformity: a report from the Scoliosis Research Society Morbidity and Mortality Committee. Spine (Phila Pa 1976). 2011;36:958-64.

[2] Luca A, Ottardi C, Sasso M, Prosdocimo L, La Barbera L, Brayda-Bruno M, et al. Instrumentation failure following pedicle subtraction osteotomy: the role of rod material, diameter, and multi-rod constructs. Eur Spine J. 2016.

[3] Ahn HS, DiAngelo DJ. Biomechanical testing simulation of a cadaver spine specimen: development and evaluation study. Spine (Phila Pa 1976). 2007;32:E330-6.

[4] White III AA, Panjabi MM. Clinical Biomechanics of the Spine. Second Edition ed: Lippincott Williams & Wilkins; 1990.

[5] Cook DJ, Yeager MS, Cheng BC. Range of motion of the intact lumbar segment: a multivariate study of 42 lumbar spines. Int J Spine Surg. 2015;9:5.

[6] Oda IMD, Abumi KMD, Cunningham BWM, Kaneda KMDa, McAfee PCMD. An In Vitro Human Cadaveric Study Investigating the Biomechanical Properties of the Thoracic Spine. Spine. 2002;27:E64-E70.

[7] Metzger MF, Robinson ST, Svet MT, Liu JC, Acosta FL. Biomechanical Analysis of the Proximal Adjacent Segment after Multilevel Instrumentation of the Thoracic Spine: Do Hooks Ease the Transition? Global Spine J. 2016;6:335-43.

[8] Hindle RJ, Pearcy M, Cross A. Mechanical function of the human lumbar interspinous and supraspinous ligament. J Biomed Eng. 1990;12:340-4.

[9] Gillespie KA, Dickey JP. Biomechanical Role of Lumbar Spine Ligaments in flexion and extension: determination using a parallel linkage robot and a porcine model. Spine. 2004;29:1208-16.

[10] Corse MR, Renberg WC, Friis EA. In vitro evaluation of biomechanical effects of multiple hemilaminectomies on the canine lumbar vertebral column. American Journal of Veterinary Research. 2003;64:1139-45.

[11] Hansson TH, Keller TS, Spengler DM. Mechanical behavior of the human lumbar spine. II. Fatigue strength during dynamic compressive loading. J Orthop Res. 1987;5:479-87.

[12] Panjabi MM, Oxland TR, Yamamoto I, Crisco JJ. Mechanical behavior of the human lumbar and lumbosacral spine as shown by three-dimensional load-displacement curves. J Bone Joint Surg Am. 1994;76:413-24.

[13] Busscher I, van Dieen JH, Kingma I, van der Veen AJ, Verkerke GJ, Veldhuizen AG. Biomechanical Characteristics of Different Regions of the Human Spine. Spine. 2009;34:2858-64.

[14] Cristofolini L, Brandolini N, Danesi V, Juszczyk MM, Erani P, Viceconti M. Strain distribution in the lumbar vertebrae under different loading configurations. The spine journal : official journal of the North American Spine Society. 2013;13:1281-92.

[15] Danesi V, Erani P, Brandolini N, Juszczyk M, Cristofolini L. Effect of the In Vitro Boundary Conditions on the Surface Strain Experienced by the Vertebral Body in the Elastic Regime. Journal of biomechanical engineering. 2016;138:104503-1/9.

[16] Pintar FA, Yoganandan N, Pesigan M, Reinartz J, Sances JA, Cusick JF. Cervical Vertebral Strain Measurements Under Axial and Eccentric Loading. Journal of biomechanical engineering. 1995;117:474-8.

[17] Shah J, Hampson W, Jayson M. The distribution of surface strain in the cadaveric lumbar spine. J Bone Joint Surg Br. 1978;60-B:246-51.

[18] Little EG, Tocher D, O'Donnel P. Strain gauge reinforcement of plastics. Strain. 1990;26:91-8.

[19] Ajovalasit A, D'Acquisto L, Fragapane S, Zuccarello B. Stiffness and Reinforcement Effect of Electrical Resistance Strain Gauges. Strain. 2007;43:229-305.

[20] Stokes I. Surface Strain on Human Intervertebral Discs. Journal of Orthopaedic Research. 1987;5:348-55.

[21] Spera D, Genovese K, Voloshin A. Application of Stereo-Digital Image Correlation to Full-Field 3-D Deformation Measurement of Intervertebral Disc. Strain. 2011;47:e572-e87.

[22] Busscher I, Ploegmakers J, Verkerke G, Veldhuizen A. Comparative anatomical dimensions of the complete human and porcine spine. European spine journal. 2010;19:1104-14.

[23] Busscher I, van der Veen AJ, van Dieen JH, Kingma I, Verkerke GJ, Veldhuizen AG. In vitro biomechanical characteristics of the spine: a comparison between human and porcine spinal segments. Spine (Phila Pa 1976). 2010;35:E35-42.

[24] Wilke HJ, Geppert J, Kienle A. Biomechanical in vitro evaluation of the complete porcine spine in comparison with data of the human spine. Eur Spine J. 2011;20:1859-68.

[25] Rohlmann A, Neller S, Claes L, Bergmann G, Wilke HJ. Influence of a follower load on intradiscal pressure and intersegmental rotation of the lumbar spine. Spine (Phila Pa 1976). 2001;26:E557-61.

[26] Palanca M, Tozzi G, Cristofolini L. The Use Of Digital Image Correlation In The BIomechanical Field: A Review. Inter Biomech. 2016;3:1-21.

[27] Barranger Y, Doumalin P, Dupré JC, Germaneau A. Digital Image Correlation accuracy: influence of kind of speckle and recording setup. EPJ Web of Conferences. 2010;6:31002.

[28] Lionello G, Sirieix C, Baleani M. An effective procedure to create a speckle pattern on biological soft tissue for digital image correlation measurements. J Mech Behav Biomed Mater. 2014;39:1-8.

[29] Luyckx T, Verstraete M, De Roo K, De Waele W, Bellemans J, Victor J. Digital image correlation as tool for 3D strain analysis in human tendon tissue. The journal of experimental orthopedics. 2014;1.

[30] Sutton MA, Orteu JJ, Schreier HW. Image Correlation for Shape, Motion and Deformation Meaasurements. Springer Science. 2009.

[31] Brandolini N, Cristofolini L, Viceconti M. Experimental Method for the Biomechanical Investigation of Human Spine: a Review Journal Of Mechanics in Medicine and Biology. 2014;14:1430002.

[32] Cristofolini L. In vitro evidence of the structural optimization of the human skeletal bones. Journal of biomechanics. 2015;48:787-96.

[33] O'Connell GD, Vresilovic EJ, Elliott DM. Human intervertebral disc internal strain in compression: the effect of disc region, loading position, and degeneration. J Orthop Res. 2011;29:547-55.

[34] Palanca M, Brugo TM, Cristofolini L. Use of Digital Image Correlation to Understand the Biomechanics of the Vertebra. Journal Of Mechanics in Medicine and Biology. 2015;15:1540004-1/-10.

[35] Lionello G, Cristofolini L. A practical approach to optimizing the preparation of speckle patterns for digital-image correlation. Measurement Science and Technology. 2014;25:107001.

[36] Borchers N, Reinsch N, Kalm E. THe number of ribs and vertebrae in Piétrain cross: variation, heritability and effects on performance traits. J Anim Breed Genet. 2004;121:392-403.

[37] Cristofolini L, Juszczyk M, Taddei F, Viceconti M. Strain distribution in the proximal human femoral metaphysis. Proc Inst Mech Eng H. 2009;223:273-88.

[38] Field RE, Rushton N. Proximal femoral surface strain gauge analysis of a new epiphyseal prosthesis. J Biomed Eng. 1989;11:123-9.

[39] Weinans H, Blankevoort L. Reconstruction of bone loading conditions from in vivo strain measurements. Journal of biomechanics. 1995;28:739 - 44.

[40] Sobczak S, Salvia P, Dugailly PM, Lefevre P, Feipel V, Van Sint Jan S, et al. Use of embedded strain gages for the in-vitro study of proximal tibial cancellous bone deformation during knee flexion-extension movement: development, reproducibility and preliminary results of feasibility after frontal low femoral osteotomy. Journal of Orthopaedic Surgery and Research. 2011;6:1 - 10.

[41] Lanyon LE, Hampson WGJ, Goodship AE, Shah JS. Bone deformation recorded in vivo from strain gauges attached to the human tibial shaft. Acta Orthop Scand. 1975;46:256-68.

[42] Taylor JR. Growth of human intervertebral discs and vertebral bodies. J Anat. 1975;120:49-68.

[43] Wilke H, Kettler AA, Claes EL. Are Sheep Spines a Valid Biomechanical Model for Human Spines? Spine. 1997;22:2365-74.

[44] Anderson AL, McIff TE, Asher MA, Burton DC, Glattes RC. The Effect of Posterior Thoracic Spine Anatomical Structures on Motion Segment Flexion Stiffness. Spine. 2009;34:441 - 6.

[45] Shim VPW, Liu JF, Lee VS. A Technique for Dynamic Tensile Testing of Human Cervical Spine Ligaments. Experimental Mechanics. 2006;46:77-89.

[46] Gustafson H, Siegmund G, Cripton P. Comparison of Strain Rosettes and Digital Image Correlation for Measuring Vertebral Body Strain. Journal of biomechanical engineering. 2016;138:054501-1/-6.

[47] Heuer F, Wolfram U, Schmidt H, Wilke HJ. A method to obtain surface strains of soft tissues using a laser scanning device. Journal of biomechanics. 2008;41:2402-10.

[48] Holsgrove TP, Cazzola D, Preatoni E, Trewartha G, Miles AW, Gill HS, et al. An investigation into axial impacts of the cervical spine using digital image correlation. The spine journal : official journal of the North American Spine Society. 2015;15:1856-63.

[49] Malakoutian M, Volkheimer D, Street J, Dvorak MF, Wilke HJ, Oxland TR. Do in vivo kinematic studies provide insight into adjacent segment degeneration? A qualitative systematic literature review. Eur Spine J. 2015;24:1865-81.

[50] Roberts BC, Perilli E, Reynolds KJ. Application of the digital volume correlation technique for the measurement of displacement and strain fields in bone: A literature review. Journal of biomechanics. 2014;47:923-34.

[51] Palanca M, Tozzi G, Dall'Ara E, Curto M, Innocente F, Danesi V, et al. Digital Volume Correlation can be used to estimate local strains in natural and augmented vertebrae: An organ-level study. Journal of biomechanics. 2016;49:3882-90.

[52] Tozzi G, Danesi V, Palanca M, Cristofolini L. Elastic Full-Field Strain Analysis and Microdamage Progression in the Vertebral Body from Digital Volume Correlation. Strain. 2016;52:446-55.

[53] Hussein AI, Barbone PE, Morgan EF. Digital Volume Correlation for Study of the Mechanics of Whole Bones. Procedia IUTAM. 2012;4:116-25.

Captions and figures (images here are in low resolution)

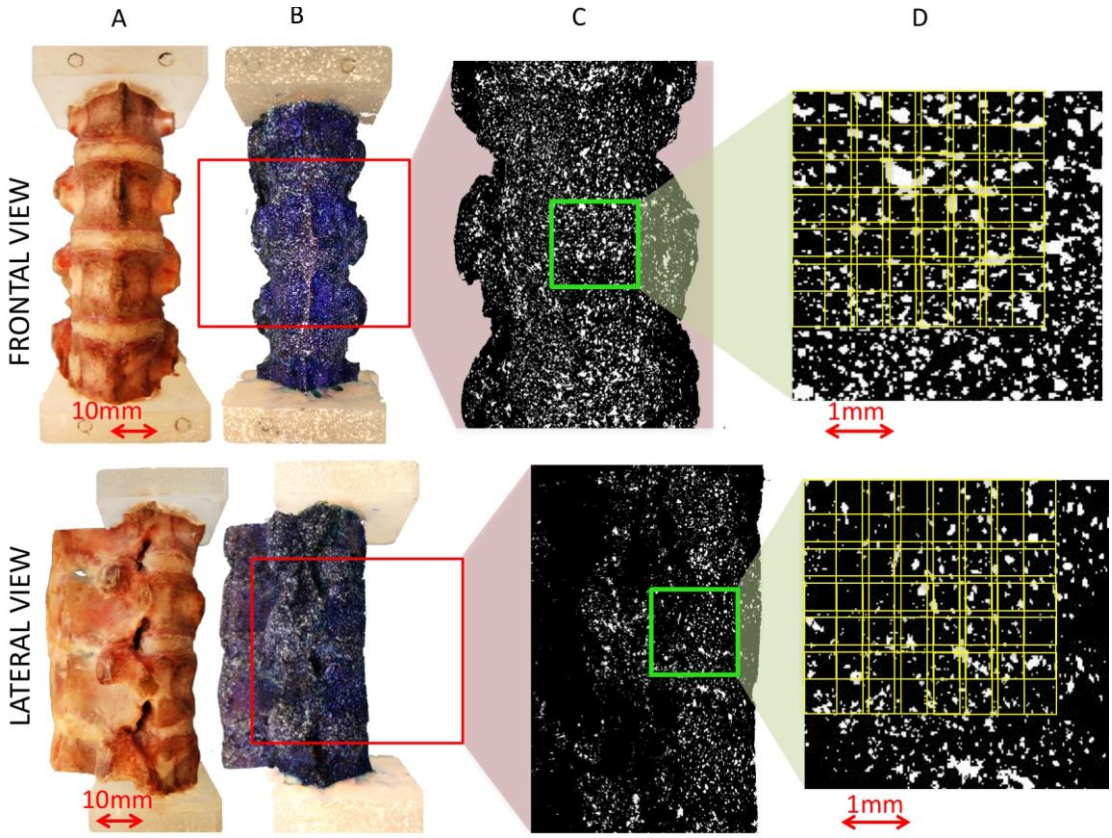

Fig. 1 - Overview at different dimensional scales of specimen preparation and analysis. The porcine spines were cleaned removing the surrounding tissues (A), and preparing the white-on-black speckle pattern (B); the red windows represent the field of view recorded by the DIC cameras. Binarized images of the entire region of interest (which covered the central disc and the two adjacent vertebrae) were generated to evaluate the dimensions of the white speckle dots (C). The facet size and grid spacing (yellow lines) can be compared to the speckle dot size in the binarized images (D).

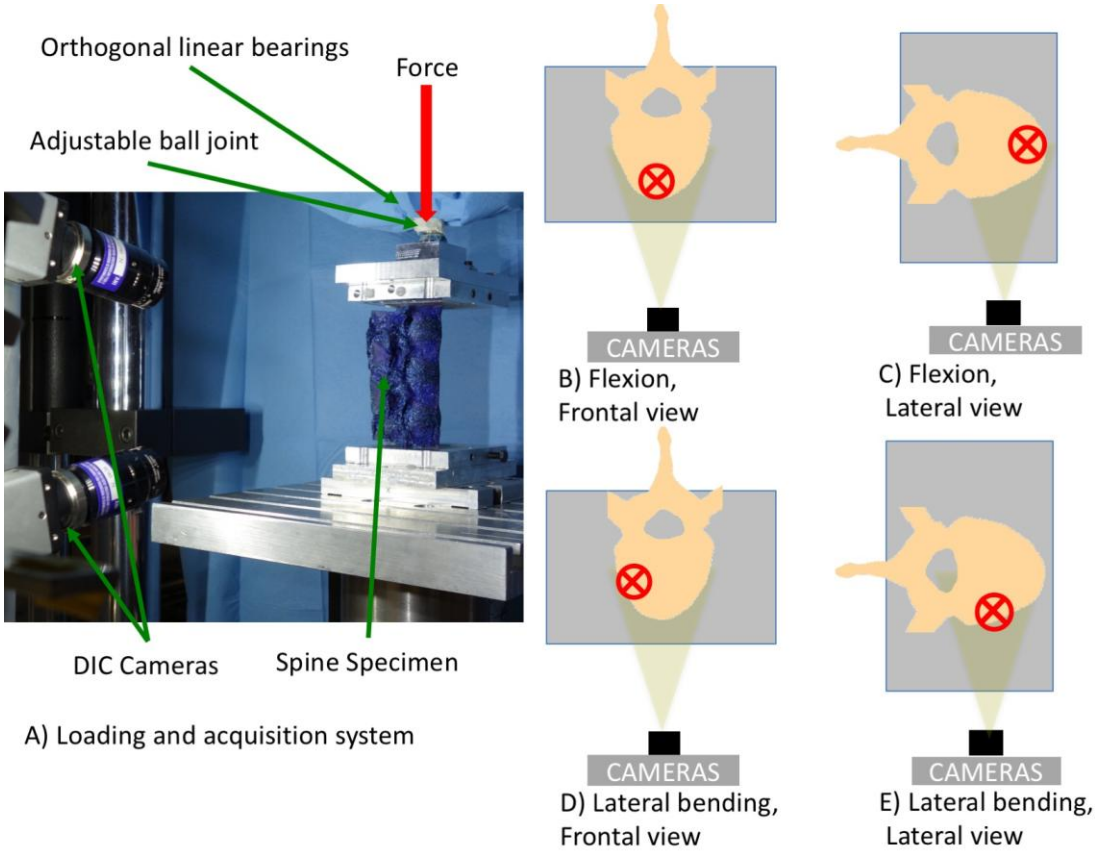

Fig. 2 - The different loading configurations were reproduced using a uniaxial testing machine and a dedicated system of low-friction linear and ball bearings to avoid transmission of undesired force components (A). The different loading configurations (flexion (B, C), lateral bending (both right and left directions were tested; the instance shown here is towards right) (D, E)) and the different views (frontal (B, D), lateral (C, E)) are sketched, viewed from top: the red cross represents the compressive force applied to the specimen. The two cameras are aligned in this top view.

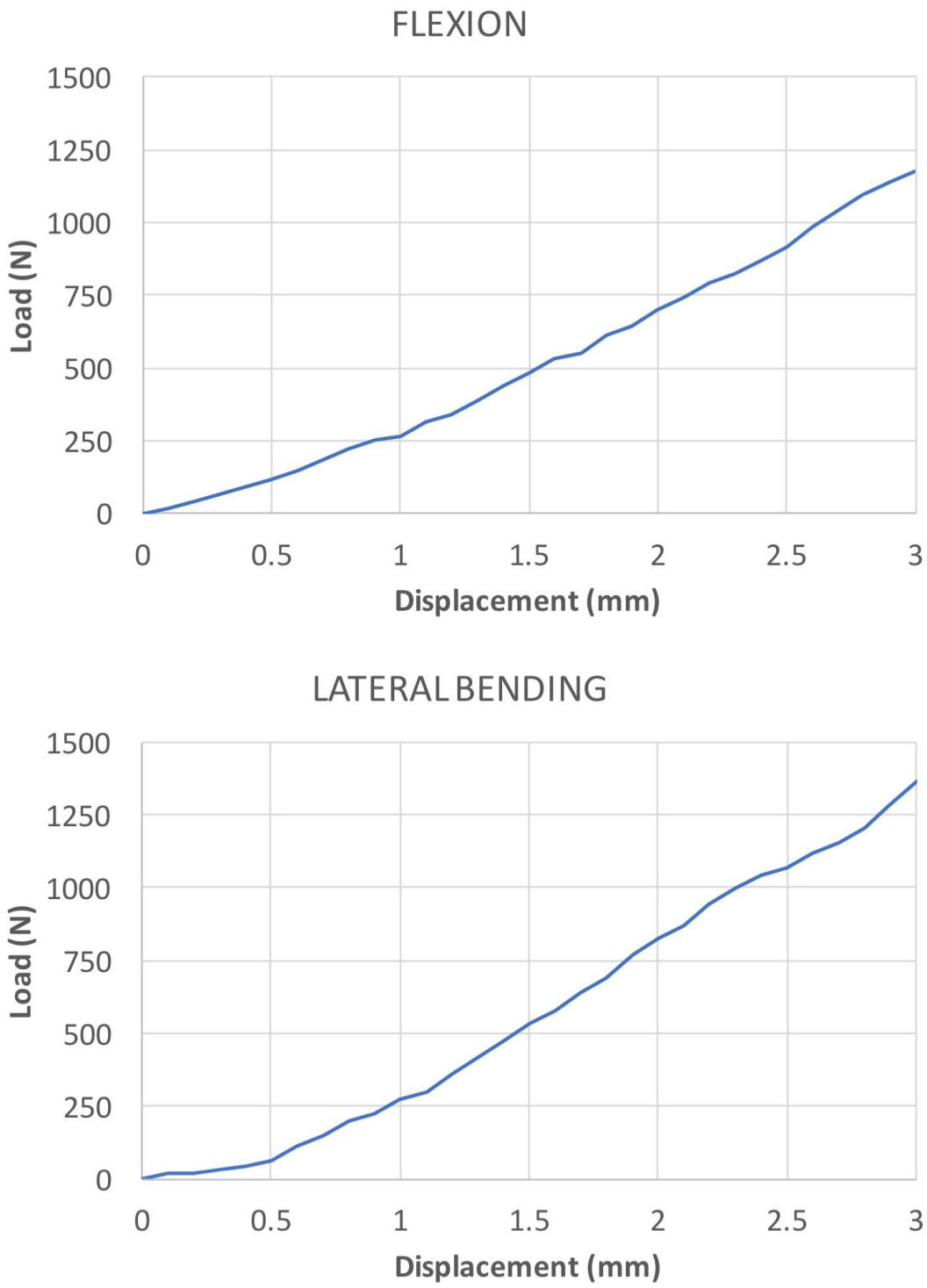

Fig. 3 – Typical Load-Displacement plot for flexion and lateral bending. The plot for one of the three specimen is represented (T11-T14): all specimens exhibited similar, rather linear, trends. The maximum load in flexion ranged between 624 N and 1956 N; for lateral bending the maximum load ranged from 566 N to 2361 N.

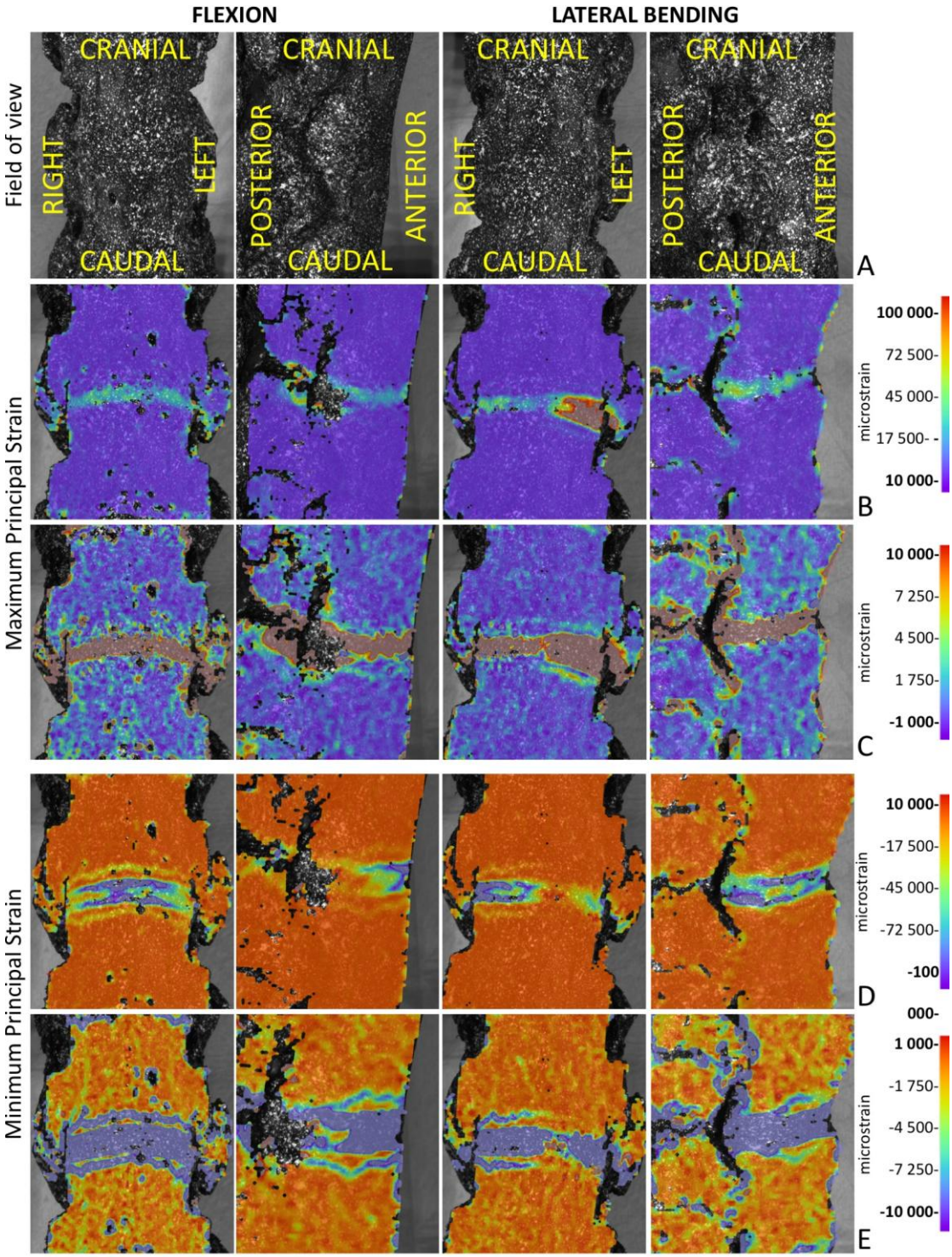

Fig. 4 - Results for a spine segment for flexion (images on the left) and for lateral bending (images on the right), both in the frontal and lateral view. The results for lateral bending with compression on the right side of the spine are shown; results for bending in the opposite direction were quite similar. The images as recorded by the DIC system are shown (A). The maps of the maximum (B, C) and minimum (D, E) principal strain are reported for the last step of the test (compression of 3 mm). As the strain in the intervertebral disc and in the vertebral bone exhibited different orders of magnitude, the strain distributions are shown twice: with a full-scale suitable for the disc (B, D) and for the vertebra (C, E). For brevity, results are shown only for one of the three specimens. The magnitude (ranges of strain observed) and distribution (localization of the strain peaks) were similar in all three specimens.

Tables

Table 1: Summary of the systematic and random errors evaluated in the anterior and lateral views for the maximum tensile (ε_1) and maximum compressive (ε_2) strains. The median and ranges over three specimens are reported.

VIEWS	**STRAINS**	**SYSTEMATIC ERRORS Median (min-max) [microstrain]**	**RANDOM ERRORS Median (min-max) [microstrain]**
Anterior	ε_1	30 (0-60)	90 (40-90)
	ε_2	-10 (-70-0)	90 (60-100)
Sagittal	ε_1	5 (0-50)	140 (90-170)
	ε_2	-10 (-30-10)	140 (70-180)

Full-field strain distribution in multi-vertebra spine segments:

An *in vitro* application of Digital Image Correlation

Marco Palanca
School of Engineering and Architecture, Alma Mater Studiorum – Università di Bologna
Via Terracini 28, 40131, Bologna (Italy)
marco.palanca2@unibo.it

Miguel Marco
Department of Mechanical Engineering, Universidad Carlos III de Madrid
Avd. de la Universidad, 30. 28911 Leganés (Madrid) España
mimarcoe@ing.uc3m.es

Maria Luisa Ruspi
School of Engineering and Architecture, Alma Mater Studiorum – Università di Bologna
Via Terracini 28, 40131, Bologna (Italy)
marialuisa.ruspi2@unibo.it

Luca Cristofolini*
Department of Industrial Engineering, School of Engineering and Architecture, Alma Mater Studiorum – Università di Bologna
Viale Risorgimento 2, 40136, Bologna (Italy)
luca.cristofolini@unibo.it

*Corresponding author

Abstract

The biomechanics of the spine is experimentally assessed in terms of range of motion and overall stiffness. Quantification of the surface strain distribution is currently limited either to the vertebrae or the discs, whereas a full-field approach to measure the strain distribution in a multi-vertebra segment is currently missing. The aim of this work was to explore the feasibility of using Digital Image Correlation (DIC) to measure the strain distribution simultaneously on the vertebral bodies and the intervertebral discs of spine segments in different loading configurations.

Three porcine spine segments were tested. A white-on-black speckle pattern was prepared which covered the hard and soft tissues. Two different loading configurations (flexion and lateral bending) were reproduced, while two sides of the spine were analyzed with DIC.

Measurements were successfully performed on the entire region of interest of all specimens, in both configurations. The DIC analysis highlighted the strain gradients present on the spine segments including tension and compression associated with bending, the direction of principal strains in the different regions, as well as bulging of the discs under compression. Strains of tens of thousands microstrain were measured in the discs, and below 2000 microstrain in the bone.

This work showed the feasibility of applying DIC on spine segments including hard and soft tissues. It also highlights the need for a full-field investigation, because of the strain inhomogeneity in the vertebrae and discs.

Keywords: Biomechanics; Spine segment; Full-field strain measurement with Digital Image Correlation; Feasibility study; Intervertebral Discs; Vertebrae.

1. Introduction

The spine consists in a sequence of hard (vertebrae) and soft tissue (intervertebral discs), stabilized by ligaments. Spine characterization is a fundamental challenge in biomechanics because it could help engineers and clinicians to better understand physiological/pathological conditions, and to design better implants [1, 2].

Spine segments have often been investigated *in vitro* [3-7]. In such experiments either known motions are imposed to measure the structural stiffness [8-10], or known loads are applied to measure the range of motion[11-13]. From these tests, structural properties and behaviour of the spine segment as a whole is assessed. Only in few cases the local strain distribution has been measured. However, such experiments focused separately either on the vertebra or on the intervertebral disc. Strain in the vertebra has been measured by means of strain gauges [14-17]; this provided accurate measurements, but was limited to the area of application of the strain gauges. The reinforcement effect of strain gauges can be significant (up to 9%) [14, 18, 19]. Measuring the local strain in the intervertebral disc is even more difficult, due to the intrinsic nature of the disc itself (low stiffness). One of the first measurements of the strain on the outer part of the disc (*annulus fibrosus*) was based on stereo-photogrammetry and covered a limited portion of the disc [20]. More recently, the entire disc surface was investigated (excluding the adjacent vertebrae), using digital image correlation (DIC) [21]. A method to explore the strain field on spine segments with large in-plane and out-of-plane deformations is missing.

The aim of this work was to explore the feasibility of using DIC to measure the full-field strain distribution simultaneously on the vertebral bodies and intervertebral discs of thoracolumbar spine segments in different loading configurations. Specifically, the following research questions were addressed:

- The feasibility of applying a speckle pattern with sufficient contrast for the correlation algorithm, that should not become damaged when the specimen was kept hydrated;

- The robustness of the pattern to withstand the large deformations expected in the soft tissue (up to 100000 microstrain) for up to 50 cycles;
- The procedure must allow measuring the small deformations expected in bone (of the order of 2000 microstrain) with acceptable errors (not exceeding 200 microstrain);
- The possibility of measuring strains in specimens undergoing relatively large in-plane (up to 3 mm) and out-of-plane (7 mm) displacements, while correlating at least 90% of the region of interest.

2. Material and methods

2.1 Specimen and pattern preparation

For ethical reasons, in this methodological work porcine spine segments from the slaughterhouse were preferred. The three animals were female, of the same breed, approximately 9 months old and approximately 100 kg at sacrifice. The segments consisted of four thoracolumbar vertebrae (T7-T10/T11-T14/L2-L5) selected for resemblance in terms of ranges of motion and dimensions [22-24]. The specimens were kept hydrated, and stored at -28°C to avoid alteration of the mechanical properties.

The ribs, the muscles, the anterior longitudinal ligament, and the periosteum were carefully removed using surgical tools. The interspinous, supraspinous and posterior longitudinal ligaments, and the capsules were left intact in order to preserve the natural kinematics. The specimens were aligned so that the middle disc of each segment was aligned horizontally in the frontal and lateral views [25]. In this configuration, two pots of poly-methyl-methacrylate were created parallel to one another, where the upper half of the most cranial vertebra and the lower half of the most caudal vertebra, were embedded (Fig. 1).

In order to use DIC to make measurement on the spine segments (both the vertebrae and the intervertebral discs), a high-contrast white-on-black speckle pattern [26, 27] was prepared. The spine segments were first stained with a dark background (a solution of 4 g of methylene-blue per 100 ml of water) [28, 29]. Two applications were required for the intervertebral discs and three for

the vertebrae to obtain a uniform background. Dying was preferred, rather than surface painting, as a layer of paint would crumble and crack due to the large deformations of the soft tissues.

The speckle pattern was applied with paint instead of using a powder, as was done previously [26]. This allows avoiding artifacts as the dots can strain during the test (unlike powder grains). Furthermore, paint dots resist to saline solution without damage, allowing specimen hydration and storage. A white water-based paint (Q250201 Bianco Opaco, Chrèon, Italy) was diluted at 40% with water and sprayed using an airbrush-airgun (AZ3 HTE 2, nozzle 1.8 mm, Antes Iwata, Italy) to prepare a white speckle pattern with the qualitative and quantitative requirements described in [30]. The spraying distance (300 mm) and the pressure (1000 kPa) were optimized to obtain the desired dot size, and minimize the scatter of dot dimension [35]. The actual size of the speckle dots was measured in the 2D digital images (acquired by DIC system) of the ROI through a custom script developed for this work. The speckles had a dimension of 6 pixels (average 0.18 mm with a standard deviation of 0.18 mm), larger than the minimum recommended size while the facet were sufficiently large compared to the speckle size [30].

The specimens were soaked in saline solution before the tests.

2.2 Mechanical Testing

The specimens were loaded using a uniaxial servo-hydraulic testing machine (8032, Instron, UK) in displacement control. In order to avoid transmission of any undesired component of load, free rotation of the loading plate was allowed by means of a ball joint, while free horizontal translations were granted by means of two low-friction orthogonal linear bearings.

In order to assess the feasibility of measuring strains on such complex specimens, two different loading configurations were simulated, which are frequently investigated in the literature [31] (Fig. 2):

- Flexion: the vertical force had an anterior offset equal to the 20% of the antero-posterior depth of the central intervertebral disc;

- Lateral bending: the vertical force had a lateral offset (both towards right and left) equal to the 20% of the coronal width of the central intervertebral disc.

Ten preconditioning cycles were applied between 0 and 1.0 mm of compression, at 0.5 Hz. A compression of 3.0 mm was applied for each loading configuration in 0.1 mm steps, while DIC images were acquired at each step (see below). This value of compression was based on preliminary tests to reach typical strains associate to physiological loads [32, 33] to prevent damage of the specimens. These loading configurations did not aim to mimic any specific motor task.

2.3 Digital Image Correlation

A commercial 3D-DIC system (Q400, Dantec Dynamics, Denmark) with directional custom designed arrays of LEDs (10000 lumen in total) was used. Images were acquired by two cameras (5MegaPixels, 2440x2050 pixels, 8-bit) equipped with high-quality metrology-standard 35 mm lens (Apo-Xenoplan 1.8/35, Schneider-Kreuznach, Germany; 135 mm equivalent) for a stereoscopic view. Due to the curvature of the vertebral bodies and discs, the cameras were positioned at a distance of 260 mm from the specimen and vertically to maximize the area framed by both cameras (Fig. 2).

The field of view was set to 70 mm by 60 mm (resulting in a pixel size of 28 micrometers), with depth of field of 20 mm (lens aperture f/16). The field of view was wide enough to frame the entire region of interest (ROI): the central intervertebral disc and the two adjacent vertebrae.

To explore the possibility of assessing the different sides of the spine, two different acquisitions were performed for each loading configuration and each specimen:

- Frontal view: the cameras pointed the anterior wall of the spine segment;
- Lateral view: the cameras pointed the lateral side (either right or left) of the spine segment.

During the mechanical tests, series of images were acquired starting from the unloaded condition (reference step) and every 0.1 mm step of compression.

The correlation was performed with Istra-4D (v.4.3.1, Dantec Dynamics, Denmark) using the following parameters (Fig. 1):

a) Facet size: 33 pixels;
b) Grid spacing: 19 pixels;
c) Contour smoothing: local regression with a kernel size of 5x5;

It is not possible to exactly quantify the measurement spatial resolution due to the nonlinearity of the smoothing process. With the settings used, a spatial resolution better than 3 mm was estimated (comparable with the typical dimension of the strain gauges used in biomechanical field [14]).

Finally, the maximum (ε_1) and minimum (ε_2) principal strains were evaluated.

2.4 Optimization and error analysis

As DIC relies on a complex preparation, acquisition and analysis, its accuracy and precision cannot be taken from granted. We capitalized on past experience on optimization of pattern preparation [28] [35], image acquisition and correlation parameters [34] (see 2.1 and 2.3).
Before each session, calibration was performed using a proprietary calibration target (Mod. Al4-BMB-9x9, Dantec Dynamics): 3D-residuum values from 0.031 to 0.173. It is a proprietary procedure and it consists in acquiring a series of images of the target calibration in different orientations to define the physical dimensions of the measurement volume, the correction of the distortions due to lens and the compensation of the parallax effects.

An optimization and validation of the system was preliminarily performed [34] to find the best compromise between the uncertainties and DIC parameters. A pair of images of the unloaded segments were captured for each specimen and analyzed with the optimal hardware and software settings in order to assess the measurement uncertainties in a known configuration (zero-strain). Being in a zero-strain configuration, any strain different from zero was accounted as measurement error. The Kolmogorov-Smirnov test was used to check that the errors followed a Gaussian distribution. The systematic and random errors [34] were computed for each specimen and for each view as the average and the standard deviation of ε_1 and ε_2.

3. Results

Measurements were successfully performed on all specimens, over the entire region of interest in both the frontal and sagittal view, for both loading configurations, during the entire tests. Similar strain distributions were found in the three specimens. The different tissues were easily identified observing the physical specimens and the images acquired by the cameras. The evolution of the strain distribution during load application (Fig. 3) is visible in the videos in the Supplementary Material.

3.1 Strain error

In the zero-strain test, the apparent strains followed a Gaussian distribution (Kolmogorov-Smirnov). As expected, the largest component of error was the random error, and it never exceeded 190 microstrain.

3.2 Flexion – Frontal view

During flexion, at most 4.4% (worst specimen) of the ROI in the frontal view lost correlation between the first and the last step. The discs underwent larger deformations compared to the vertebral bone (Fig. 4). The strain in the discs followed a strain gradient, with peaks in the central portion. In the discs, ε_1 was on the order of +20000 microstrain (aligned circumferentially) and ε_2 was of the order of -40000 microstrain (aligned axially).

The vertebrae had lower strains: peak on the order of +500 microstrain for the ε_1 and around -1500 microstrain for ε_2. The two regions cranial and caudal to the intervertebral discs with larger strain show the large deformation of the growth plates.

3.3 Flexion – lateral view

During flexion, at most 5.7% (worst specimen) of the ROI in the lateral view lost correlation between the first and the last step. The discs presented a strain gradient: they were more deformed in tension in the posterior than in the anterior side (Fig. 4). ε_1 on the intervertebral discs varied between +12000

180 microstrain (anterior side) and +87000 microstrain (posterior side). ε_2 followed
181 a similar gradient, from -87000 microstrain (anterior) to -18000 microstrain
182 (posterior). The direction of ε_1 changed from circumferential (anterior side), to
183 axial (posterior). Therefore, in flexion the discs tended to bulge in the anterior
184 part, and to stretch in the posterior side.

185 The vertebral body experienced lower strains: below +600 microstrain for ε_1 and
186 -1500 microstrain for ε_2.

187 ***3.4 Lateral bending – frontal view***

188 During lateral bending, at most 1.5% (worst specimen) of the ROI in the frontal
189 view lost correlation between the first and the last step. Lateral bending was
190 applied both towards the right and the left sides, to all specimens: the outputs, in
191 terms of strain distribution on intervertebral discs and vertebrae were
192 symmetrical. The discs showed tension and compression respectively on the left
193 and right sides, depending on the direction of the imposed bending (Fig. 4). ε_1
194 varied between +6000 microstrain (compressed side) and +143000 microstrain
195 (stretched side). ε_2 were varied from -85000 microstrain (compressed side) to
196 +12000 microstrain (stretched side). The orientation of ε_1 changed from
197 circumferential on the compressed side, to axial on the stretched side.

198 The vertebrae had lower strains than the discs: ε_1 were lower than 500
199 microstrain and ε_2 did not exceed -1700 microstrain. In this configuration, as in
200 flexion, it was possible to observe both tension (ε_1 aligned with the vertebral
201 axis) and compression (ε_2 circumferentially) in the growth plates.

202 ***3.5 Lateral bending – lateral view***

203 During lateral bending, at most 5.2% (worst specimen) of the ROI in the lateral
204 view lost correlation between the first and the last step. The strains on the discs
205 were rather uniformly distributed compared with the other tests (Fig.4). When
206 the side in compression was observed, ε_1 in the disc were of the order of +40000
207 microstrain, and ε_2 of the order of -60000 microstrain.

The vertebral body had lower strains than the discs: ε_1 were lower than 700 microstrain and the ε_2 did not exceed -1400 microstrain.

4. Discussion

The main aim of this work was to develop a procedure to measure the strain distribution on thoracolumbar spine segments [36] simultaneously on hard tissues (the vertebrae) and soft tissues (the intervertebral discs) by means 3D-DIC [30]. Two different loading configurations frequently found in the literature [6, 11-13] were explored. The specimens were observed both frontally and laterally.

The results of this work showed the technical feasibility of quantifying the full-field strain distribution (small and large deformations) over multi-vertebra spine segments during the mechanical tests. The measured strain distributions proved to be highly inhomogeneous, confirming the importance of investigating the spine using a full-field tool to complement the evaluation of the range of motion and stiffness performed in the past.

The correlation was satisfactory throughout the tests, even if large deformations and displacements were involved. The correlated surface covered the ROI, with a loss of correlation lower than 5.7% of the initial correlated surface. Generally, the noise originating from the camera sensors, sub-optimal speckle dots, poor illumination, and bad speckle framing can contribute to loss of correlation. Here, the leakage of fluids from the vertebral body under load, which is an inherent phenomenon when testing fresh tissue, increased the loss of correlation. Additionally, the out-of-plane movements (7 mm) of the postero-lateral elements (capsule) caused some subsets to be out-of-focus in the lateral view. While DIC often has some un-correlated gaps, other measurement techniques such as strain gauges simply measure strains in selected points, and ignore the rest of the surface.

The prepared white-on-black pattern confirmed its suitability both for hard and soft tissues [28]. In fact, the background, prepared with methylene-blue, did not

crack during the tests, while the white dots remained sharp and adherent to the specimen's surface.

A compromise was sought between reduction of measurement uncertainty and spatial resolution. The hardware (camera resolution, lenses, field of view) and software parameters (facet size, grid spacing, contour smoothing) provided a measurement spatial resolution better then 3 mm. This is comparable with the grid length of the strain gauges typically used in these applications (1-5 mm) [37-40]. The strain measurement uncertainties (below 180 microstrain) were acceptable for biomechanical purposes. Such uncertainties would not prevent detecting failure of the bone (around 10000 microstrain [32]), as well as strain associated to physiological loads (1000-2000 microstrain [41]). The same considerations are confirmed for the intervertebral discs: as the failure strain is around 250000 microstrain [20], and the physiological strain is below 150000 microstrain [33].

The evaluated strains confirmed the expected trends in all performed tests: larger strains were measured in the intervertebral discs (in the order tens thousands microstrain), lower strains in the vertebrae (below 2000 microstrain). Such strain gradients are consistent with the expected biomechanics of the spine [4]. DIC discriminated the portion of the discs subjected to tension/compression, with the expected orientation of the principal strains. In the compressed side of the discs the minimum principal strains were axial, as expected; the maximum principal strains were larger in absolute value than the minimum ones, and had a transversal orientation.

The combination of the prepared pattern, selected software parameters, and hardware allowed recognizing the deformation on the growth plates of the vertebrae. Because of the spine specimens came from skeletally immature animals [42] the growth plates were not closed and therefore were subjected to larger deformation compared to the vertebral body. This was serendipity and would otherwise be impossible to observe with traditional surface measurement technique such as strain gauges.

Usually, *in vitro* spine segments have been investigated in terms of range of intersegmental motion [6, 12, 13, 43] and overall stiffness [11, 13, 44, 45]. In other works, the spine was investigated measuring local deformation either in the vertebrae or in the intervertebral discs. In the vertebrae, strains have been evaluated using strain gauges, which provide point-wise measurements. At the same time, strain gauges do cause reinforcement, especially on thin osteoporotic tissues [14, 15]. Otherwise, the vertebrae have been studied using DIC but without evaluating the contiguous discs [34, 46]. Conventional strain gauges cannot be used on the discs due to their low elastic modulus. Strain measurement is possible with optical methods [20, 21]. In the work of Stokes *et al.* [20] the deformation on a small portion of the intervertebral disc was evaluated by photogrammetry adhering small optical markers. Heuer *et al*. [47] developed a method based on laser scanning device to evaluate the strain distribution on intervertebral discs. In this case, the strain uncertainty (<1600 microstrain) would not allow measuring strain on hard tissue as vertebra. Moreover, the duration of the scan (4 seconds), constrains the applicability to quasi-static applications. In the work of Spera *et al*. [21] strain was measured only on the discs using DIC. They used coffee powder: as the coffee grains themselves are not deformable as the paint-dots, this can result in large noise, apparent strain and loss of correlation.

A work [48] focused on the strain distribution on spine segments. High-speed 3D-DIC was used to evaluate the strains on the anterior side of porcine cervical spine segments in axial impacts. In contrast, the present work aims to explore the feasibility of the measurement under large deformation, directed out-of-plane.

A limitation of this work could be the use of young porcine spine instead of human spine. This choice was motivated by ethical considerations. The porcine spines are different from the human ones but are valid models [22, 24] to demonstrate the feasibility of this novel approach.

In this work, a quite standard but relatively simple configuration of 3D-DIC was used. Array of cameras can be used to acquire 360° of the whole spine in order to obtain a complete description of the strain maps.

The applied loading configurations were not intended to replicate any specific physiological motor task, but included separate components of load which are present in physiological motor tasks (flexion and lateral bending) and which are typically found in spine biomechanics [31] as main causes of spine degeneration [49]. This study did not cover other types of loading such as torsion.

The strains were evaluated only on the surface of the specimens. Digital Volume Correlation (DVC) [50] has the potentiality to evaluate the strain within the vertebral bone [51-53]. Nevertheless, applicability of DVC is limited due to the slow tomographic image acquisition.

5. Conclusion

This work showed that by applying an adequate speckle pattern and selecting optimal DIC parameters, the full-field strain distribution could be evaluated on a complex structure (soft and hard tissues) such as a spine segment. This full-field measurement would allow assessing the strain distribution, determining the alignment of principal strains, and identify stress concentrators. This opens the way to a new method of investigation of the spine, involving new possible applications for basic biomechanics research and clinical innovations. DIC-based experimental measurements could be combined with numerical models in an inverse approach to measure (identify) the local tissue properties, including anisotropy. Furthermore, the use of DIC will help elucidate the damage and failure mechanism of the spine. DIC can also be used to investigate and improve different surgical techniques and spine fixation devices.

Conflict of Interest Statement

None

Acknowledgements

The authors would like to thank Remo Antelli for donating the porcine spines, Thorsten Siebert (Dantec Dynamics, Denmark) for the support with DIC software, and the students for the help in the preparation of the specimens (Kamila Ożóg, Büşra Savaş, Alessio Amicone).

Competing interests:

None declared

Funding:

None

Ethical approval:

Tissue specimens (porcine spines) were obtained as a side-product through the food chain from animals that have been bred and sacrificed for alimentation purposes. No animal was specifically bred or sacrificed for this study. The Biomechanics laboratory at UNIBO meets all the Italian regulations concerning research, safety in the working environment, handling, storing, testing and disposal of animal and human tissue samples. All the research was carried out in accordance with the National and local regulations guidelines and, in accordance with the EU Directive 2010/63/EU.

Bibliography

[1] Smith JS, Sansur CA, Donaldson WF, 3rd, Perra JH, Mudiyam R, Choma TJ, et al. Short-term morbidity and mortality associated with correction of thoracolumbar fixed sagittal plane deformity: a report from the Scoliosis Research Society Morbidity and Mortality Committee. Spine (Phila Pa 1976). 2011;36:958-64.

[2] Luca A, Ottardi C, Sasso M, Prosdocimo L, La Barbera L, Brayda-Bruno M, et al. Instrumentation failure following pedicle subtraction osteotomy: the role of rod material, diameter, and multi-rod constructs. Eur Spine J. 2016.

[3] Ahn HS, DiAngelo DJ. Biomechanical testing simulation of a cadaver spine specimen: development and evaluation study. Spine (Phila Pa 1976). 2007;32:E330-6.

[4] White III AA, Panjabi MM. Clinical Biomechanics of the Spine. Second Edition ed: Lippincott Williams & Wilkins; 1990.

[5] Cook DJ, Yeager MS, Cheng BC. Range of motion of the intact lumbar segment: a multivariate study of 42 lumbar spines. Int J Spine Surg. 2015;9:5.

[6] Oda IMD, Abumi KMD, Cunningham BWM, Kaneda KMDa, McAfee PCMD. An In Vitro Human Cadaveric Study Investigating the Biomechanical Properties of the Thoracic Spine. Spine. 2002;27:E64-E70.

[7] Metzger MF, Robinson ST, Svet MT, Liu JC, Acosta FL. Biomechanical Analysis of the Proximal Adjacent Segment after Multilevel Instrumentation of the Thoracic Spine: Do Hooks Ease the Transition? Global Spine J. 2016;6:335-43.

[8] Hindle RJ, Pearcy M, Cross A. Mechanical function of the human lumbar interspinous and supraspinous ligament. J Biomed Eng. 1990;12:340-4.

[9] Gillespie KA, Dickey JP. Biomechanical Role of Lumbar Spine Ligaments in flexion and extension: determination using a parallel linkage robot and a porcine model. Spine. 2004;29:1208-16.

[10] Corse MR, Renberg WC, Friis EA. In vitro evaluation of biomechanical effects of multiple hemilaminectomies on the canine lumbar vertebral column. American Journal of Veterinary Research. 2003;64:1139-45.

[11] Hansson TH, Keller TS, Spengler DM. Mechanical behavior of the human lumbar spine. II. Fatigue strength during dynamic compressive loading. J Orthop Res. 1987;5:479-87.

[12] Panjabi MM, Oxland TR, Yamamoto I, Crisco JJ. Mechanical behavior of the human lumbar and lumbosacral spine as shown by three-dimensional load-displacement curves. J Bone Joint Surg Am. 1994;76:413-24.

[13] Busscher I, van Dieen JH, Kingma I, van der Veen AJ, Verkerke GJ, Veldhuizen AG. Biomechanical Characteristics of Different Regions of the Human Spine. Spine. 2009;34:2858-64.

[14] Cristofolini L, Brandolini N, Danesi V, Juszczyk MM, Erani P, Viceconti M. Strain distribution in the lumbar vertebrae under different loading configurations. The spine journal : official journal of the North American Spine Society. 2013;13:1281-92.

[15] Danesi V, Erani P, Brandolini N, Juszczyk M, Cristofolini L. Effect of the In Vitro Boundary Conditions on the Surface Strain Experienced by the Vertebral Body in the Elastic Regime. Journal of biomechanical engineering. 2016;138:104503-1/9.

[16] Pintar FA, Yoganandan N, Pesigan M, Reinartz J, Sances JA, Cusick JF. Cervical Vertebral Strain Measurements Under Axial and Eccentric Loading. Journal of biomechanical engineering. 1995;117:474-8.

[17] Shah J, Hampson W, Jayson M. The distribution of surface strain in the cadaveric lumbar spine. J Bone Joint Surg Br. 1978;60-B:246-51.

[18] Little EG, Tocher D, O'Donnel P. Strain gauge reinforcement of plastics. Strain. 1990;26:91-8.

[19] Ajovalasit A, D'Acquisto L, Fragapane S, Zuccarello B. Stiffness and Reinforcement Effect of Electrical Resistance Strain Gauges. Strain. 2007;43:229-305.

[20] Stokes I. Surface Strain on Human Intervertebral Discs. Journal of Orthopaedic Research. 1987;5:348-55.

[21] Spera D, Genovese K, Voloshin A. Application of Stereo-Digital Image Correlation to Full-Field 3-D Deformation Measurement of Intervertebral Disc. Strain. 2011;47:e572-e87.

[22] Busscher I, Ploegmakers J, Verkerke G, Veldhuizen A. Comparative anatomical dimensions of the complete human and porcine spine. European spine journal. 2010;19:1104-14.

[23] Busscher I, van der Veen AJ, van Dieen JH, Kingma I, Verkerke GJ, Veldhuizen AG. In vitro biomechanical characteristics of the spine: a comparison between human and porcine spinal segments. Spine (Phila Pa 1976). 2010;35:E35-42.

[24] Wilke HJ, Geppert J, Kienle A. Biomechanical in vitro evaluation of the complete porcine spine in comparison with data of the human spine. Eur Spine J. 2011;20:1859-68.

[25] Rohlmann A, Neller S, Claes L, Bergmann G, Wilke HJ. Influence of a follower load on intradiscal pressure and intersegmental rotation of the lumbar spine. Spine (Phila Pa 1976). 2001;26:E557-61.

[26] Palanca M, Tozzi G, Cristofolini L. The Use Of Digital Image Correlation In The BIomechanical Field: A Review. Inter Biomech. 2016;3:1-21.

[27] Barranger Y, Doumalin P, Dupré JC, Germaneau A. Digital Image Correlation accuracy: influence of kind of speckle and recording setup. EPJ Web of Conferences. 2010;6:31002.

[28] Lionello G, Sirieix C, Baleani M. An effective procedure to create a speckle pattern on biological soft tissue for digital image correlation measurements. J Mech Behav Biomed Mater. 2014;39:1-8.

[29] Luyckx T, Verstraete M, De Roo K, De Waele W, Bellemans J, Victor J. Digital image correlation as tool for 3D strain analysis in human tendon tissue. The journal of experimental orthopedics. 2014;1.

[30] Sutton MA, Orteu JJ, Schreier HW. Image Correlation for Shape, Motion and Deformation Meaasurements. Springer Science. 2009.

[31] Brandolini N, Cristofolini L, Viceconti M. Experimental Method for the Biomechanical Investigation of Human Spine: a Review Journal Of Mechanics in Medicine and Biology. 2014;14:1430002.

[32] Cristofolini L. In vitro evidence of the structural optimization of the human skeletal bones. Journal of biomechanics. 2015;48:787-96.

[33] O'Connell GD, Vresilovic EJ, Elliott DM. Human intervertebral disc internal strain in compression: the effect of disc region, loading position, and degeneration. J Orthop Res. 2011;29:547-55.

[34] Palanca M, Brugo TM, Cristofolini L. Use of Digital Image Correlation to Understand the Biomechanics of the Vertebra. Journal Of Mechanics in Medicine and Biology. 2015;15:1540004-1/-10.

[35] Lionello G, Cristofolini L. A practical approach to optimizing the preparation of speckle patterns for digital-image correlation. Measurement Science and Technology. 2014;25:107001.

[36] Borchers N, Reinsch N, Kalm E. THe number of ribs and vertebrae in Piétrain cross: variation, heritability and effects on performance traits. J Anim Breed Genet. 2004;121:392-403.

[37] Cristofolini L, Juszczyk M, Taddei F, Viceconti M. Strain distribution in the proximal human femoral metaphysis. Proc Inst Mech Eng H. 2009;223:273-88.

[38] Field RE, Rushton N. Proximal femoral surface strain gauge analysis of a new epiphyseal prosthesis. J Biomed Eng. 1989;11:123-9.

[39] Weinans H, Blankevoort L. Reconstruction of bone loading conditions from in vivo strain measurements. Journal of biomechanics. 1995;28:739 - 44.

[40] Sobczak S, Salvia P, Dugailly PM, Lefevre P, Feipel V, Van Sint Jan S, et al. Use of embedded strain gages for the in-vitro study of proximal tibial cancellous bone deformation during knee flexion-extension movement: development, reproducibility and preliminary results of feasibility after frontal low femoral osteotomy. Journal of Orthopaedic Surgery and Research. 2011;6:1 - 10.

[41] Lanyon LE, Hampson WGJ, Goodship AE, Shah JS. Bone deformation recorded in vivo from strain gauges attached to the human tibial shaft. Acta Orthop Scand. 1975;46:256-68.

[42] Taylor JR. Growth of human intervertebral discs and vertebral bodies. J Anat. 1975;120:49-68.

[43] Wilke H, Kettler AA, Claes EL. Are Sheep Spines a Valid Biomechanical Model for Human Spines? Spine. 1997;22:2365-74.

[44] Anderson AL, McIff TE, Asher MA, Burton DC, Glattes RC. The Effect of Posterior Thoracic Spine Anatomical Structures on Motion Segment Flexion Stiffness. Spine. 2009;34:441 - 6.

[45] Shim VPW, Liu JF, Lee VS. A Technique for Dynamic Tensile Testing of Human Cervical Spine Ligaments. Experimental Mechanics. 2006;46:77-89.

[46] Gustafson H, Siegmund G, Cripton P. Comparison of Strain Rosettes and Digital Image Correlation for Measuring Vertebral Body Strain. Journal of biomechanical engineering. 2016;138:054501-1/-6.

[47] Heuer F, Wolfram U, Schmidt H, Wilke HJ. A method to obtain surface strains of soft tissues using a laser scanning device. Journal of biomechanics. 2008;41:2402-10.

[48] Holsgrove TP, Cazzola D, Preatoni E, Trewartha G, Miles AW, Gill HS, et al. An investigation into axial impacts of the cervical spine using digital image correlation. The spine journal : official journal of the North American Spine Society. 2015;15:1856-63.

[49] Malakoutian M, Volkheimer D, Street J, Dvorak MF, Wilke HJ, Oxland TR. Do in vivo kinematic studies provide insight into adjacent segment degeneration? A qualitative systematic literature review. Eur Spine J. 2015;24:1865-81.

[50] Roberts BC, Perilli E, Reynolds KJ. Application of the digital volume correlation technique for the measurement of displacement and strain fields in bone: A literature review. Journal of biomechanics. 2014;47:923-34.

[51] Palanca M, Tozzi G, Dall'Ara E, Curto M, Innocente F, Danesi V, et al. Digital Volume Correlation can be used to estimate local strains in natural and augmented vertebrae: An organ-level study. Journal of biomechanics. 2016;49:3882-90.

[52] Tozzi G, Danesi V, Palanca M, Cristofolini L. Elastic Full-Field Strain Analysis and Microdamage Progression in the Vertebral Body from Digital Volume Correlation. Strain. 2016;52:446-55.

[53] Hussein AI, Barbone PE, Morgan EF. Digital Volume Correlation for Study of the Mechanics of Whole Bones. Procedia IUTAM. 2012;4:116-25.

Captions and figures (images here are in low resolution)

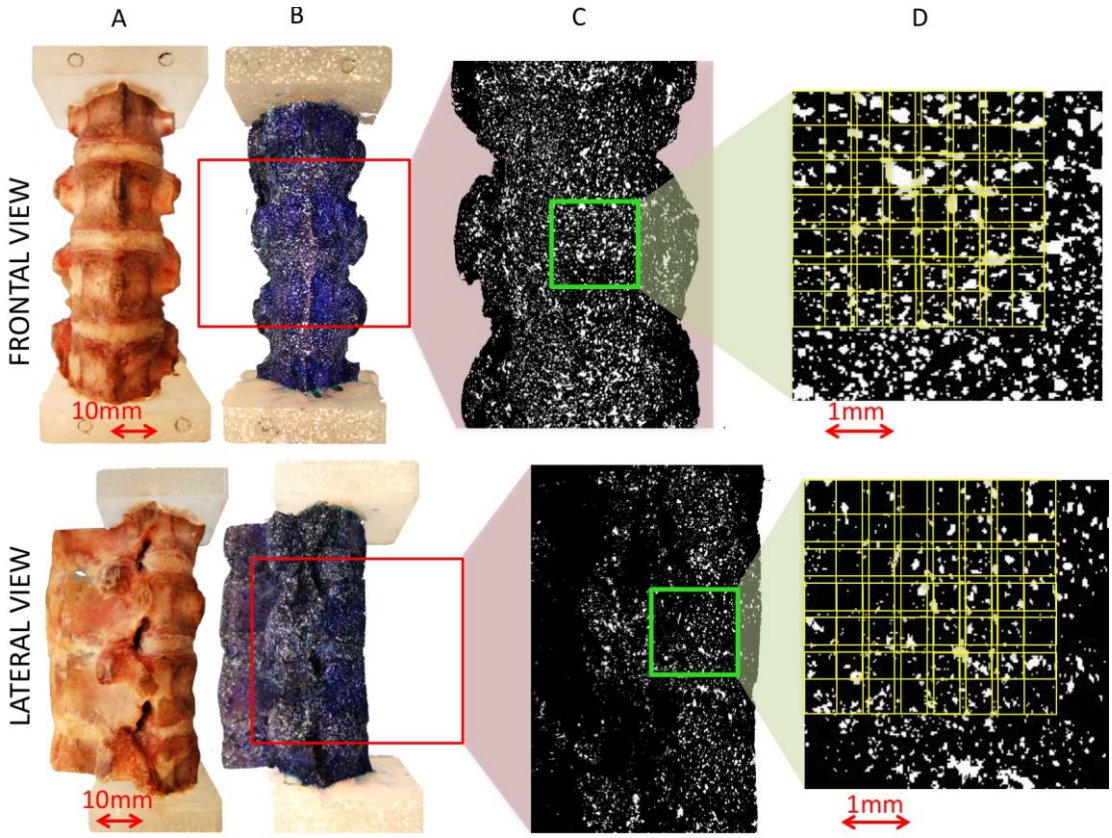

Fig. 1 - Overview at different dimensional scales of specimen preparation and analysis. The porcine spines were cleaned removing the surrounding tissues (A), and preparing the white-on-black speckle pattern (B); the red windows represent the field of view recorded by the DIC cameras. Binarized images of the entire region of interest (which covered the central disc and the two adjacent vertebrae) were generated to evaluate the dimensions of the white speckle dots (C). The facet size and grid spacing (yellow lines) can be compared to the speckle dot size in the binarized images (D).

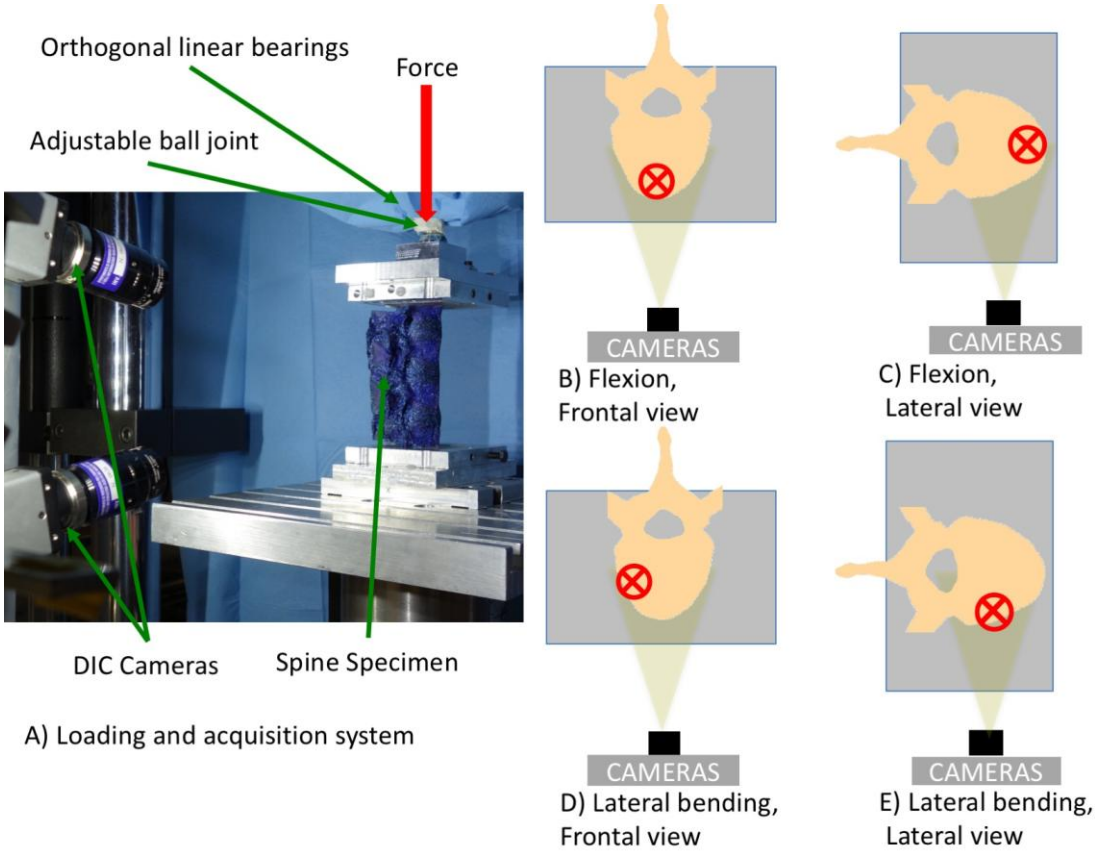

Fig. 2 - The different loading configurations were reproduced using a uniaxial testing machine and a dedicated system of low-friction linear and ball bearings to avoid transmission of undesired force components (A). The different loading configurations (flexion (B, C), lateral bending (both right and left directions were tested; the instance shown here is towards right) (D, E)) and the different views (frontal (B, D), lateral (C, E)) are sketched, viewed from top: the red cross represents the compressive force applied to the specimen. The two cameras are aligned in this top view.

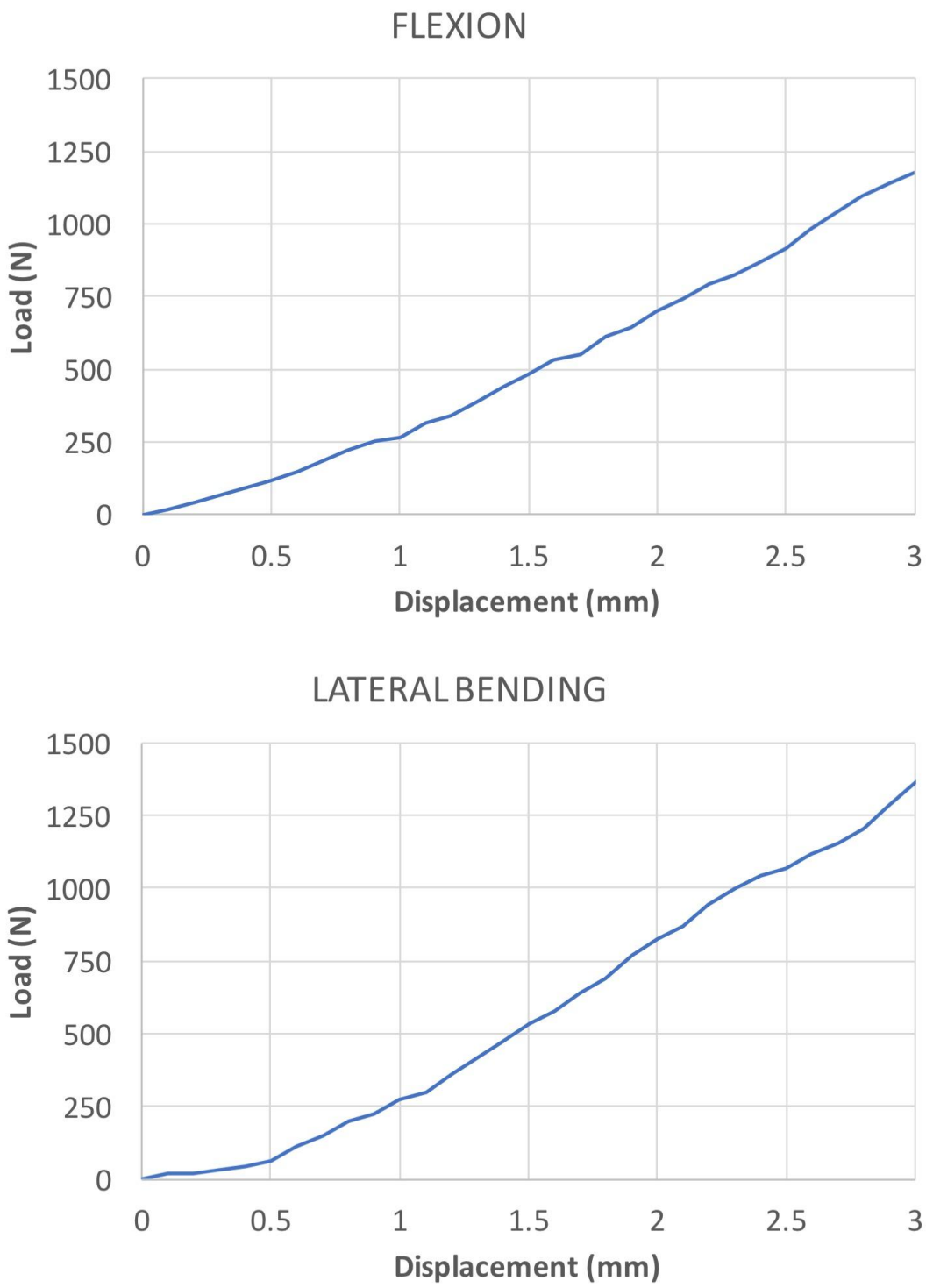

Fig. 3 – Typical Load-Displacement plot for flexion and lateral bending. The plot for one of the three specimen is represented (T11-T14): all specimens exhibited similar, rather linear, trends. The maximum load in flexion ranged between 624 N and 1956 N; for lateral bending the maximum load ranged from 566 N to 2361 N.

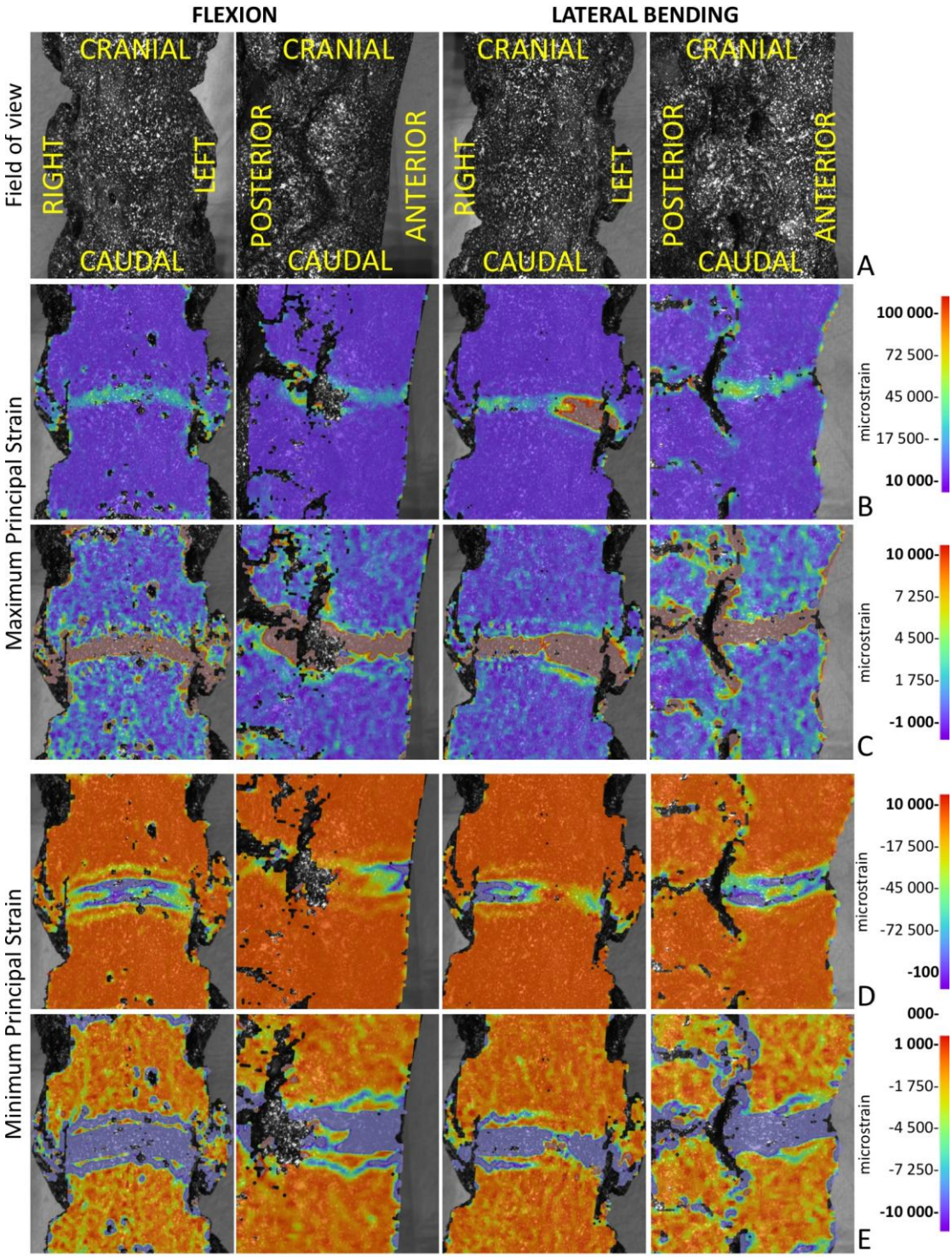

Fig. 4 - Results for a spine segment for flexion (images on the left) and for lateral bending (images on the right), both in the frontal and lateral view. The results for lateral bending with compression on the right side of the spine are shown; results for bending in the opposite direction were quite similar. The images as recorded by the DIC system are shown (A). The maps of the maximum (B, C) and minimum (D, E) principal strain are reported for the last step of the test (compression of 3 mm). As the strain in the intervertebral disc and in the vertebral bone exhibited different orders of magnitude, the strain distributions are shown twice: with a full-scale suitable for the disc (B, D) and for the vertebra (C, E). For brevity, results are shown only for one of the three specimens. The magnitude (ranges of strain observed) and distribution (localization of the strain peaks) were similar in all three specimens.

Tables

Table 1: Summary of the systematic and random errors evaluated in the anterior and lateral views for the maximum tensile (ε_1) and maximum compressive (ε_2) strains. The median and ranges over three specimens are reported.

VIEWS	STRAINS	SYSTEMATIC ERRORS Median (min-max) [microstrain]	RANDOM ERRORS Median (min-max) [microstrain]
Anterior	ε_1	30 (0-60)	90 (40-90)
	ε_2	-10 (-70-0)	90 (60-100)
Sagittal	ε_1	5 (0-50)	140 (90-170)
	ε_2	-10 (-30-10)	140 (70-180)

Fig_1

Click here to download high resolution image

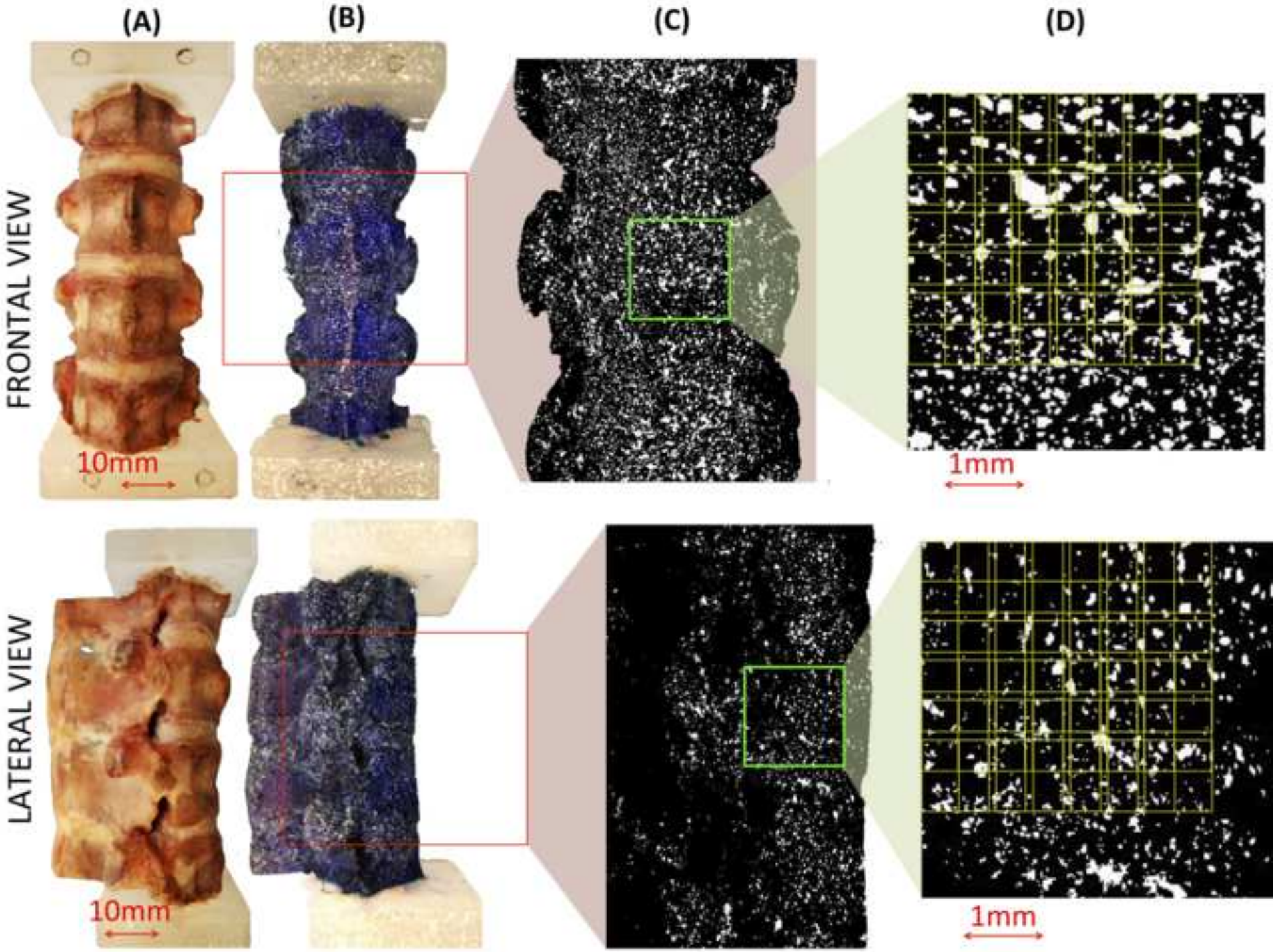

Fig_2
Click here to download high resolution image

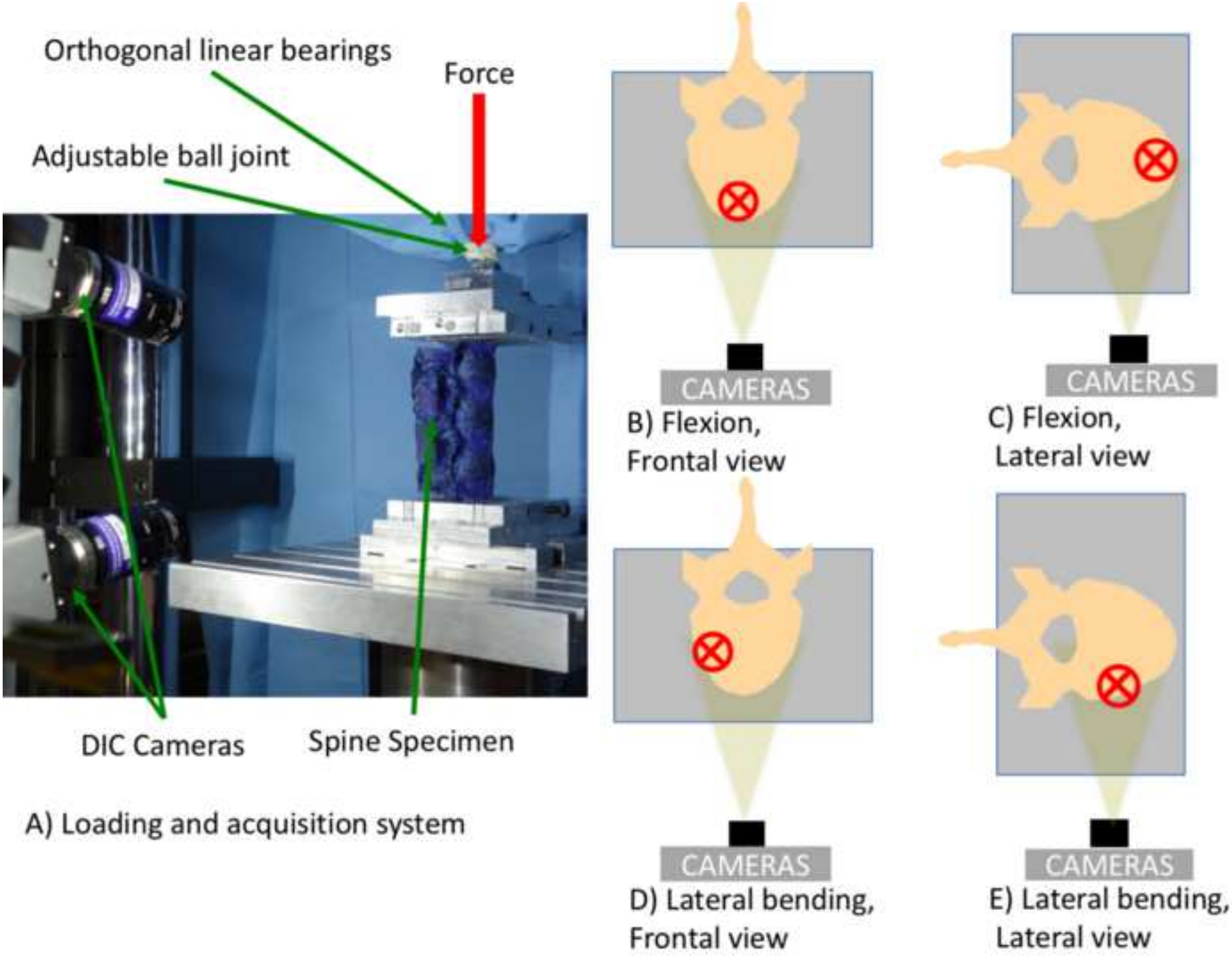

Fig_3
Click here to download high resolution image

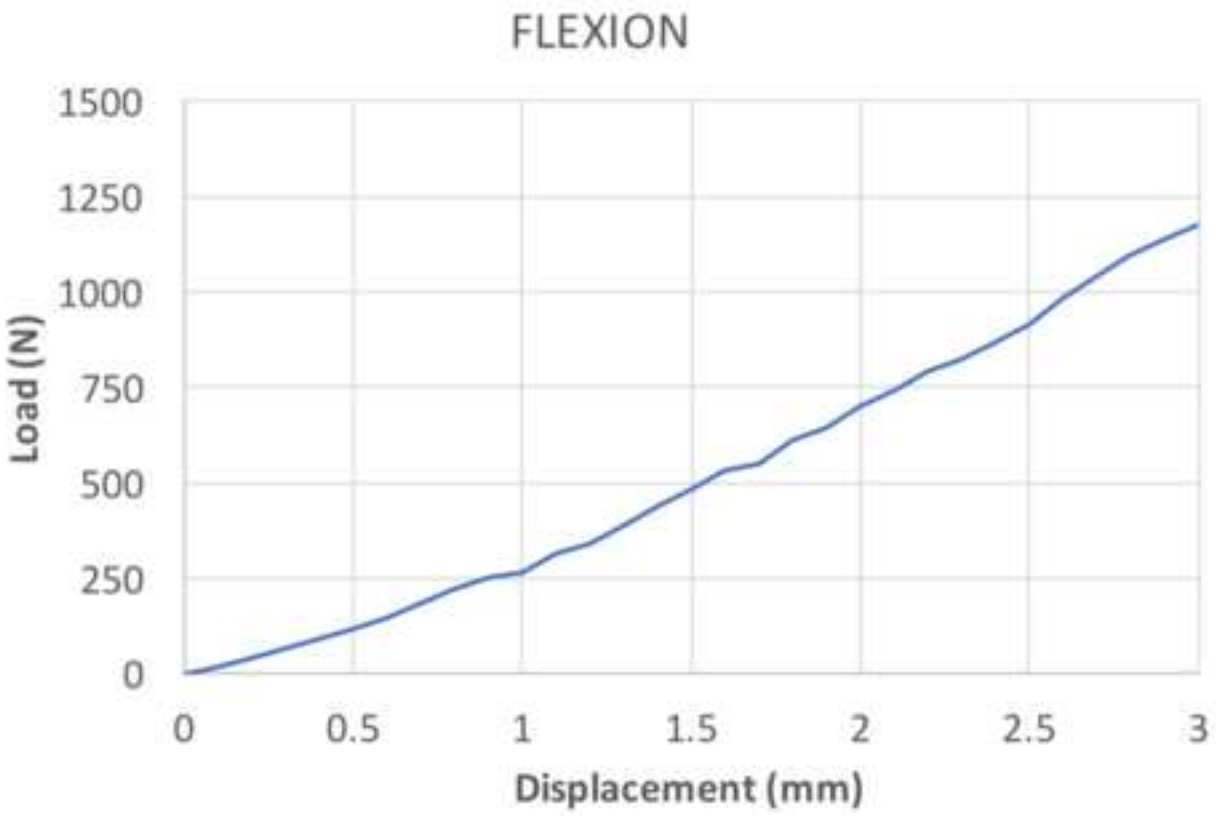

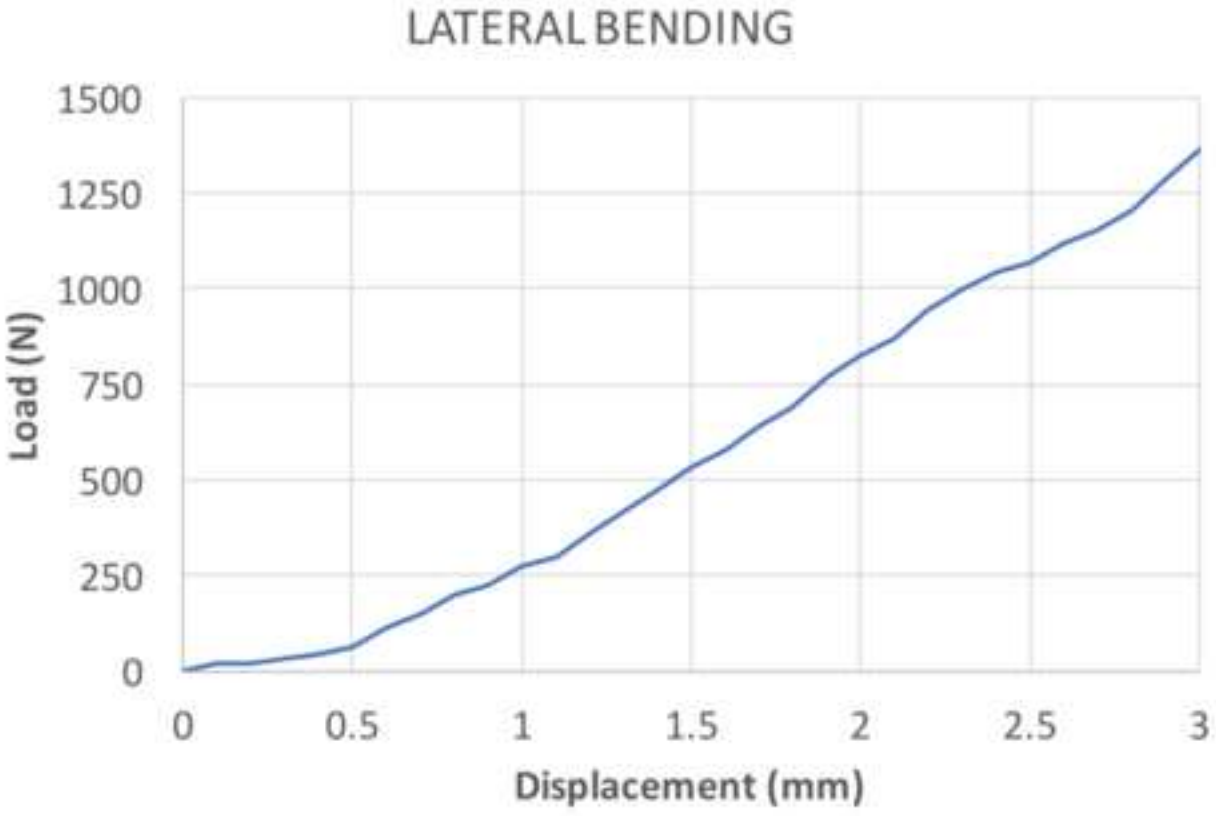

Fig_4

Click here to download high resolution image

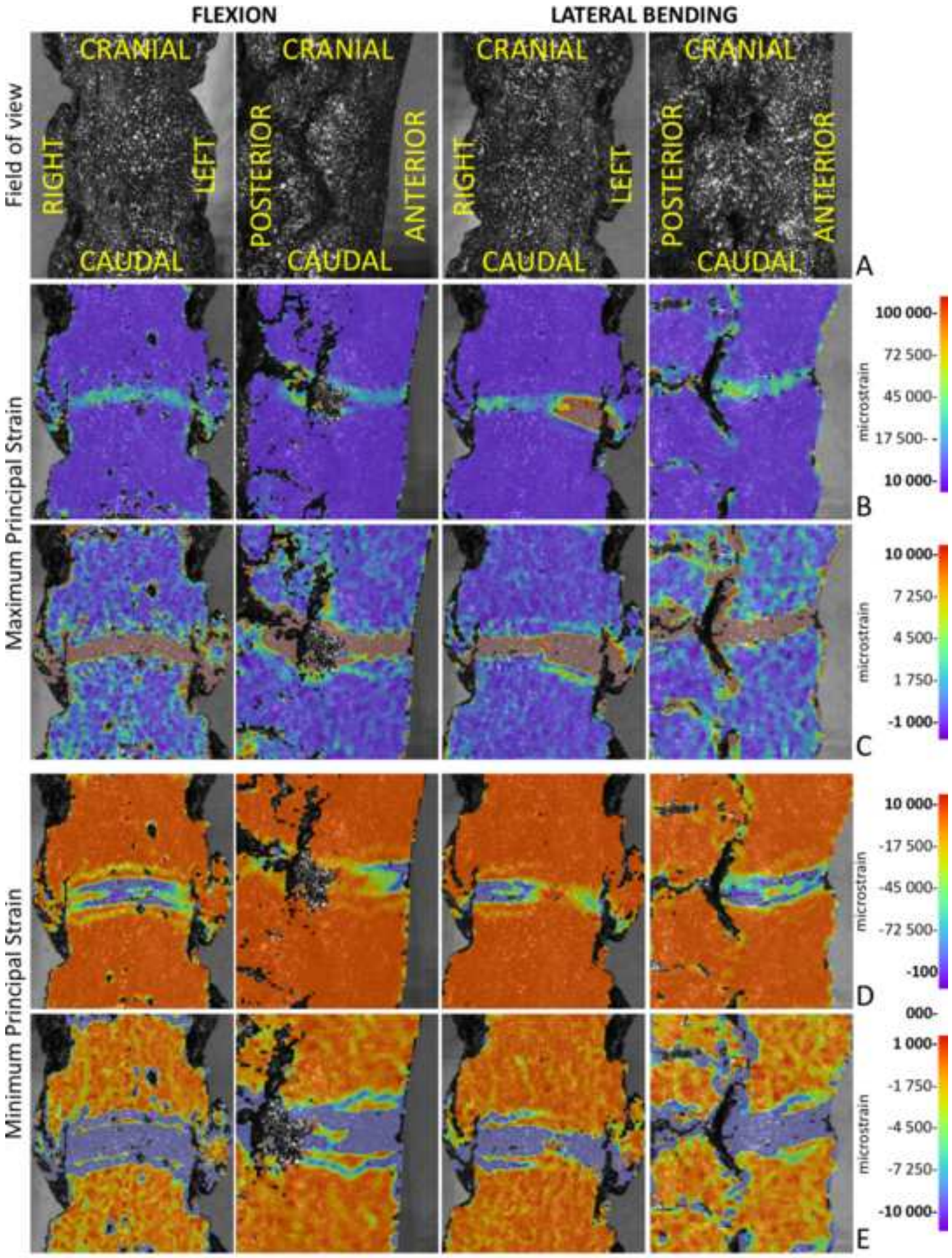

Supplementary data

Click here to download Supplementary data: _aaa_Explanatory_file_for_attached_movies.pdf

Supplementary data

Click here to download Supplementary data: 1_max_ab_fv.avi

Supplementary data

Click here to download Supplementary data: 2_min_ab_fv.avi

Supplementary data

Click here to download Supplementary data: 3_max_ab_lv.avi

Supplementary data

Click here to download Supplementary data: 4_min_ab_lv.avi

Supplementary data

Click here to download Supplementary data: 5_max_lb_fv.avi

Supplementary data

Click here to download Supplementary data: 6_min_lb_fv.avi

Supplementary data

Click here to download Supplementary data: 7_max_lb_lv.avi

Supplementary data

Click here to download Supplementary data: 8_min_lb_lv.avi